HHS Public Access

Author manuscript

Nature. Author manuscript; available in PMC 2017 September 09.

Published in final edited form as:

Nature. 2017 March 09; 543(7644): 252–256. doi:10.1038/nature21379.

Survival of tissue-resident memory T cells requires exogenous lipid uptake and metabolism

Youdong Pan[1], **Tian Tian**[1], **Chang Ook Park**[1], **Serena Y. Lofftus**[1], **Shenglin Mei**[2], **Xing Liu**[3], **Chi Luo**[4], **John T. O'Malley**[1], **Ahmed Gehad**[1], **Jessica E. Teague**[1], **Sherrie J. Divito**[1], **Robert Fuhlbrigge**[1], **Pere Puigserver**[4], **James G. Krueger**[5], **Gökhan S. Hotamisligil**[6], **Rachael A. Clark**[1,7], and **Thomas S. Kupper**[1,7]

[1]Department of Dermatology and Harvard Skin Disease Research Center, Brigham and Women's Hospital, Boston, Harvard Medical School, Boston, Massachusetts, USA

[2]Department of Biostatistics and Computational Biology, Center for Functional Epigenetics, Dana-Farber Cancer Institute, Boston, Massachusetts, USA

[3]Program in Cellular and Molecular Medicine, Boston Children's Hospital, Department of Pediatrics, Harvard Medical School, Boston, Massachusetts, USA

[4]Department of Cancer Biology. Dana Farber Cancer Institute, Department of Cell Biology, Harvard Medical School, Boston, Massachusetts, USA

[5]Department of Dermatology, Rockefeller University, New York, New York, USA

[6]Harvard T.H. Chan School of Public Health, Boston, Massachusetts, USA

[7]Dana-Farber/Brigham and Women's Cancer Center, Boston, Massachusetts, USA

Abstract

Tissue-resident memory T (T_{RM}) cells persist indefinitely in epithelial barrier tissues and protect the host against pathogens[1–4]. However, the biological pathways that enable the long-term survival of T_{RM} cells are obscure[4,5]. Here we show that mouse $CD8^+$ T_{RM} cells generated by viral infection of the skin differentially express high levels of several molecules that mediate lipid uptake and intracellular transport, including fatty-acid-binding proteins 4 and 5 (FABP4 and FABP5). We further show that T-cell-specific deficiency of *Fabp4* and *Fabp5* (*Fabp4*/*Fabp5*) impairs exogenous free fatty acid (FFA) uptake by $CD8^+$ T_{RM} cells and greatly reduces their long-term survival *in vivo*, while having no effect on the survival of central memory T (T_{CM}) cells in lymph nodes. *In vitro*, $CD8^+$ T_{RM} cells, but not $CD8^+$ T_{CM}, demonstrated increased mitochondrial

Correspondence and requests for materials should be addressed to T.S.K (tkupper@bwh.harvard.edu).

Author Contributions Y.P. and T.S.K. conceived the project, designed experiments and analysed the data. Y.P., T.T., C.O.P., S.Y.L., X.L., J.T.O. and A.G. performed the experiments and helped to analyse the data. J.T.O., A.G., J.E.T., J.G.K. and R.A.C helped with human skin sample collection, processing, experiments, and data analysis. S.M. helped to analyse the microarray data. C.L. and P.P. helped with Seahorse metabolism experiments. S.J.D., R.F. and G.S.H. helped with mice experiments and analysing data. Y.P. and T.S.K. wrote the manuscript.

The authors declare no competing financial interests. Readers are welcome to comment on the online version of the paper.

Reviewer Information *Nature* thanks F. Carbone and the other anonymous reviewer(s) for their contribution to the peer review of this work.

oxidative metabolism in the presence of exogenous FFAs; this increase was not seen in *Fabp4/Fabp5* double-knockout CD8$^+$ T_{RM} cells. The persistence of CD8$^+$ T_{RM} cells in the skin was strongly diminished by inhibition of mitochondrial FFA β-oxidation *in vivo*. Moreover, skin CD8$^+$ T_{RM} cells that lacked *Fabp4/Fabp5* were less effective at protecting mice from cutaneous viral infection, and lung *Fabp4/Fabp5* double-knockout CD8$^+$ T_{RM} cells generated by skin vaccinia virus (VACV) infection were less effective at protecting mice from a lethal pulmonary challenge with VACV. Consistent with the mouse data, increased FABP4 and FABP5 expression and enhanced extracellular FFA uptake were also demonstrated in human CD8$^+$ T_{RM} cells in normal and psoriatic skin. These results suggest that FABP4 and FABP5 have a critical role in the maintenance, longevity and function of CD8$^+$ T_{RM} cells, and suggest that CD8$^+$ T_{RM} cells use exogenous FFAs and their oxidative metabolism to persist in tissue and to mediate protective immunity.

Memory T cells protect the host through rapid recall responses to pathogens. A population of memory T cells that is vital for host defence, T_{RM} cells, has recently been characterized[1–4]. T_{RM} cells reside in epithelial barrier tissues and persist for long periods of time at the interface between host and environment[3,4]. Upon re-infection, CD8$^+$ T_{RM} cells provide a rapid antigen-specific immune response, creating an inflammatory and antiviral microenvironment that facilitates pathogen elimination[6–9]. Although previous studies have yielded clues[10–13], little is known about the molecular program that regulates the long-term survival of these cells. To answer this question, we first evaluated skin T_{RM} cell maturation by comparing gene expression patterns at different time points after infection. OT-I transgenic mouse T cells were transferred into recipient mice one day before immunization with a recombinant VACV that expresses chicken ovalbumin peptide (amino acid 257–264) under the control of an early gene promoter (rVACV$_{OVA}$). OT-I cells were readily found in the skin at day 5 after infection and reached their maximum level at day 10, before beginning to decrease in numbers (Extended Data Fig. 1a). Skin-infiltrating OT-I cells were sorted at different time points after infection and were analysed by transcriptional profiling. Principal-component analysis showed that transcriptomes of skin-infiltrating T cells clustered tightly from day 25 to day 90 after infection, suggesting that mouse skin CD8$^+$ T_{RM} cell maturation is largely completed by day 25 after infection (Fig. 1a). Transcriptomes of T_{RM} cells are distinct from those of central memory T (T_{CM}) cells and effector memory T (T_{EM}) cells (Fig. 1a, b and Extended Data Fig. 1b), consistent with previous reports[11–13]. Next, we directly compared T_{RM} cells (day 30) and T_{CM} cells (Fig. 1c). Notably, genes encoding FABP4 and FABP5 were among the most strongly upregulated genes in T_{RM} cells, as was the gene that encodes CD36, a lipid-scavenger cell-surface receptor[15] (Fig. 1c). Quantitative real-time PCR (qPCR) confirmed the increased gene expression of *Fabp4* and *Fabp5* in CD8$^+$ T_{RM} cells (Fig. 1d, e and Extended Data Fig. 1c). Immunofluorescence staining of the skin showed expression of FABP4 and FABP5 in skin CD8$^+$ T_{RM} cells (Fig. 1f). To extend these observations to other peripheral tissues, mice with transferred OT-I cells were infected with VACV$_{OVA}$ by intratracheal infection and gene expression of *Fabp4* and *Fabp5* was measured 30 days later in lung CD8$^+$ T_{RM} cells. Consistently, increased *Fabp4* and *Fabp5* gene expression was observed (Extended Data Fig. 1d).

Peroxisome proliferator-activated receptors (PPARs) are adipogenic regulators that have been reported to influence *Fabp4* and *Fabp5* gene expression[16]. *Pparg*, but not *Ppara* or *Ppard*, was selectively upregulated in T_{RM} cells compared to naive T cells (T_N), T_{CM} and T_{EM} cells (Fig. 1g and data not shown). Knockdown of *Pparg* expression using short interfering (si)RNA lentiviruses, or by treatment of mice with GW9662 (an irreversible PPARγ antagonist), inhibited *Fabp4* and *Fabp5* gene expression in $CD8^+$ T_{RM} cells (Fig. 1h and Extended Data Fig. 1e, f). These data indicate that PPARγ is an upstream regulator of *Fabp4* and *Fabp*5 gene expression.

Upon activation, naive T cells undergo metabolic reprogramming as they proliferate and develop into different subsets of memory T cells[17,18]. The strongly upregulated T_{RM} genes *Fabp4* and *Fabp5* encode lipid chaperone proteins that bind to hydrophobic ligands, thereby coordinating lipid uptake and intracellular trafficking[19]. Extracellular FFAs could be visualized in the mouse epidermis, where skin $CD8^+$ T_{RM} cells localize[3] (Extended Data Fig. 2). Given the magnitude of their upregulation, we hypothesized that FABP4 and FABP5 might play a role in $CD8^+$ T_{RM} cell physiology in the skin. To test our hypothesis, we first compared the extracellular FFA uptake of OT-I memory T cell subtypes *in vitro*. Compared to T_N, T_{CM} and T_{EM} cells, substantially more of a green fluorescent fatty acid, Bodipy FL C_{16}, was internalized by OT-I T_{RM} cells (Fig. 2a). FABP4 and FABP5 are highly homologous and bind to fatty acids with similar selectivity and affinity[19]. Given the compensatory and redundant role of these two molecules[20], we used double-knockout mice that lacked both *Fabp4* and *Fabp5* (*Fabp4*$^{-/-}$/*Fabp5*$^{-/-}$) to analyse the contribution of these molecules to FFA uptake. FACS analysis showed that OT-I *Fabp4*$^{-/-}$/*Fabp5*$^{-/-}$ T_{RM} cells internalized substantially less fatty acids *in vitro* compared to wild-type cells (Fig. 2b), suggesting that FABP4 and FABP5 are important for the specific uptake of palmitate. We then investigated whether loss of FABP4 and FABP5 would impair T_{RM} cell behaviour *in vivo*. OT-I wild-type and OT-1 *Fabp4*$^{-/-}$/*Fabp5*$^{-/-}$ cells were mixed at a 1:1 ratio and transferred into congenic recipients. Mice were then infected with $VACV_{OVA}$, and the number of OT-I wild-type and OT-I *Fabp4*$^{-/-}$/*Fabp5*$^{-/-}$ cells in different anatomic compartments was assessed. No difference was observed between the number of spleen wild-type OT-I or OT-I *Fabp4*$^{-/-}$/*Fabp5*$^{-/-}$ T_{CM} cells at any time point, indicating that deficiency in FABP4 and FABP5 did not affect T_{CM} cell survival (Fig. 2c). However, OT-I *Fabp4*$^{-/-}$/*Fabp5*$^{-/-}$ cells in the skin displayed a marked reduction in persistence, beginning at 25 days after infection. The ratio of OT-I *Fabp4*$^{-/-}$/*Fabp5*$^{-/-}$ to OT-1 wild-type T_{RM} cells declined steadily over time thereafter (Fig. 2c). Deficiency of both FABP4 and FABP5 also decreased numbers of OT-I T_{RM} cells detectable by immunofluorescence staining without affecting their recruitment or tissue localization (Fig. 2d and Extended Data Fig. 3). By contrast, OT-1 *Fabp4*$^{-/-}$, *Fabp5*$^{-/-}$, or *Fabp4*$^{+/-}$*Fabp 5*$^{+/-}$ T_{RM} cells showed no defect in long-term survival (Extended Data Fig. 4), consistent with the compensatory and redundant role of these two proteins[20]. Highly proliferative OT-I effector T (T_{eff}) cells took up more FFAs than T_N, T_{CM} and T_{EM} cells but less than T_{RM} cells (Extended Data Fig. 5a, b). Notably, OT-I *Fabp4*$^{-/-}$/*Fabp5*$^{-/-}$ T_{eff} cells displayed a similar proliferative capacity and tissue-homing receptor expression as wild-type T_{eff} cells at 60 h after infection (Extended Data Fig. 5c). These data indicate that the absence of FABP4 and FABP5 does not affect $CD8^+$ T-cell proliferation or recruitment to the skin. Inhibition of *Fabp4*/*Fabp5* gene

expression by knocking down *Pparg* expression in OT-I cells, or inhibition of PPARγ by GW9662 treatment, decreased the long-term persistence of $CD8^+$ T_{RM} cells in the skin (Extended Data Fig. 6). These data suggest that FABP4 and FABP5 are essential for the long-term survival of $CD8^+$ T_{RM} cells in skin. Annexin-V staining of OT-I wild-type and *Fabp4*$^{-/-}$/*Fabp5*$^{-/-}$ T_{RM} cells shows that the latter had a higher rate of apoptosis (Fig. 2e). The gene-expression profile of *Fabp4*$^{-/-}$/*Fabp5*$^{-/-}$ T_{RM} cells revealed that immune-response genes were significantly downregulated, whereas genes involved in anti-inflammatory responses and apoptosis were upregulated compared to wild-type cells (Extended Data Fig. 7).

To determine the dependence of T_{RM} cells on exogenous FFA uptake for oxidative metabolism, we used the Seahorse fatty-acid oxidation assay[21]. Addition of extracellular fatty acids induced a significantly higher basal and FCCP-stimulated maximum oxygen-consumption rate (OCR) in OT-I T_{RM} cells (Fig. 2f). The increase in OCR was blocked by pre-treatment with etomoxir, an inhibitor of mitochondrial carnitine palmitoyltransferase 1a (CPT1A), an enzyme central to mitochondrial fatty acid β-oxidation[22] (Fig. 2f). By contrast, T_{CM} or *Fabp4*$^{-/-}$/*Fabp5*$^{-/-}$ T_{RM} OT-I cells did not have an increased OCR when supplied with exogenous fatty acids, and the addition of etomoxir had no effect on their cellular respiration (Fig. 2f). *In vivo* knockdown of *Cpt1a* or treatment of mice with either etomoxir or trimetazidine[23] decreased the number of OT-I wild-type T_{RM} cells to a similar extent as *Fabp4*$^{-/-}$/*Fabp5*$^{-/-}$ cells (Fig. 2g and Extended Data Fig. 8a–c). These data suggest that skin $CD8^+$ T_{RM} use oxidative metabolism of exogenous FFAs to support their long-time survival. Early after infection, roughly equivalent numbers of wild-type and *Fabp4*$^{-/-}$/*Fabp5*$^{-/-}$ $CD8^+$ T_{eff} cells were found in skin (Fig. 2c). Compared to skin T_{RM} cells isolated at day 30, skin infiltrating T_{eff} cells isolated at days 10 and 15 had a lower OCR, but a higher basal extracellular acidification rate (ECAR), which corresponds to glycolysis[21] (Extended Data Fig. 8d). Deficiency in *Fabp4*/*Fabp5* decreased the OCR of T_{RM} cells at day 30 after infection, but had no effect on the ECAR of skin-infiltrating T_{eff} cells (Extended Data Fig. 8d). These data suggest that early skin-infiltrating T_{eff} cells use glycolysis, which is unaffected by *Fabp4*/*Fabp5* gene expression.

To establish the contribution of FABP4 and FABP5 to survivalof non-transgenic $CD8^+$ T_{RM} cells, bone-marrow chimaeric mice, which have a 1:1 ratio of $Thy1.1^+$ $CD45.1^+$ wild-type and $Thy1.1^+$ $CD45.2^+$ *Fabp4*$^{-/-}$/*Fabp5*$^{-/-}$ bone-marrow cells were infected with rVACV by skin scarification. After 45 days, infected skin tissue was collected and the number of VACV-pentamer$^+$ $CD8^+$ T cells[3] was analysed by flow cytometry. Consistent with data from OT-I experiments, fewer *Fabp4*$^{-/-}$/*Fabp5*$^{-/-}$ T_{RM} cells were detected compared to wild-type T_{RM} cells (Fig. 2h).

T_{RM} cells are more effective at clearing tissue VACV infections than T_{CM} cells[3]. We evaluated the contribution of FABP4 and FABP5 to viral clearance of $CD8^+$ T_{RM} cells. Mice were adoptively transferred with OT-I wild-type or OT-I *Fabp4*$^{-/-}$/*Fabp5*$^{-/-}$ cells and then infected by skin scarification with $VACV_{OVA}$. Mice were re-challenged with $VACV_{OVA}$ 25 days later and skin viral load was measured 6 days later (Fig. 3a). FTY720, a sphingosine-1-phosphate receptor antagonist, was injected into mice to assess the contribution of circulating T_{CM} cells to viral clearance (Extended Data Fig. 9a). Established OT-I wild-type

T_{RM} cells were highly effective at clearing virus from skin, which was rapid and unaffected by FTY720 treatment (Fig. 3b). By contrast, OT-I *Fabp4*$^{-/-}$/*Fabp5*$^{-/-}$ T_{RM} cells were less effective at viral clearance, and least effective following FTY720 treatment (Fig. 3b). Treatment of mice with etomoxir reduced the VACV-clearing capacity of OT-I wild-type T_{RM} cells to a level comparable to that of *Fabp4*$^{-/-}$/*Fabp5*$^{-/-}$ cells (Fig. 3b), suggesting dependence upon oxidative metabolism of FFAs. Upon stimulation *in vitro*, OT-I *Fabp4*$^{-/-}$/*Fabp5*$^{-/-}$ T_{RM} cells displayed impaired IFNγ production compared to wild-type cells (Fig. 3c, d). Similar results were obtained for OT-I *Fabp4*$^{-/-}$/*Fabp5*$^{-/-}$ T_{RM} cells residing at skin sites distant from the infection (Extended Data Fig. 9b, c).

We showed previously that lung $CD8^+$ T_{RM} cells generated by skin VACV vaccination could partially protect mice against a lethal respiratory challenge with VACV[9]. We therefore investigated the role of FABP4 and FABP5 in this protective capacity of lung $CD8^+$ T_{RM} cells generated by skin scarification. Rag1$^{-/-}$ mice were reconstituted with transfer of $CD4^+$ and $CD8^+$ wild-type or *Fabp4*$^{-/-}$/*Fabp5*$^{-/-}$ T cells one day before immunization with rVACV by skin scarification. At day 25, wild-type or *Fabp4*$^{-/-}$/*Fabp5*$^{-/-}$ rVACV memory mice were challenged intranasally with lethal doses of the highly pathogenic Western Reserve (WR)-VACV (Fig. 3e). Mice with wild-type $CD8^+$ T_{RM} cells did not display symptoms associated with illness (for example, weight loss) (Fig. 3f). By contrast, mice with *Fabp4*$^{-/-}$/*Fabp5*$^{-/-}$ $CD8^+$ T_{RM} cells showed marked weight loss after challenge and were only partially protected from virus-induced lethality (Fig. 3f, g). Treatment with FTY720 led to 100% mortality of mice that had received *Fabp4*$^{-/-}$/*Fabp5*$^{-/-}$ $CD8^+$ T_{RM} cells, whereas animals with wild-type $CD8^+$ T_{RM} cells were partially, but significantly, protected (Fig. 3f, g). These data suggest that lung *Fabp4*$^{-/-}$/*Fabp5*$^{-/-}$ $CD8^+$ T_{RM} cells were less protective against lethal respiratory VACV infection, and required the recruitment of circulating T_{CM} cells. By contrast, wild-type $CD8^+$ T_{RM} cells alone protected 50% of mice from this lethal VACV infection, consistent with our previous data[9].

T_{RM} cells in human skin have been implicated in the pathogenesis of several human skin diseases, including psoriasis[10,24,25]. We found that FABP4 and FABP5 were both strongly expressed in human skin $CD8^+$ T_{RM} cells compared to human blood T_N, T_{CM} and T_{EM} cells using FACS analysis (Fig. 4a, b). Psoriasis is a chronic and recurring autoimmune disease (Fig. 4c) that is thought to be mediated by $CD8^+$ T_{RM} cells[5,26]. Immunofluorescence staining of lesional psoriatic skin showed a co-expression of CD8 and CD69 (ref. 5), indicating that $CD8^+$ T cells in psoriasis tissue display a T_{RM}-cell phenotype (Fig. 4d). Lipids could be visualized in lesional scalp skin (Extended Data Fig. 10) and FABP4 and FABP5 protein expression could be detected in human psoriatic skin $CD8^+$ T_{RM} cells (Fig. 4e). *In vitro* incubation with exogenous Bodipy FL C_{16} showed that human skin $CD8^+$ T_{RM} cells internalized more exogenous FFAs compared to blood T_N, T_{CM} and T_{EM} cells (Fig. 4f), suggesting a similar role for FABP4 and FABP5 in fatty-acid uptake of human $CD8^+$ T_{RM} cells as we have demonstrated in mice.

Skin and other epithelial tissues are lipid-rich but nutrient-poor microenvironments[15,27], and $CD8^+$ T_{RM} cells appear to use mitochondrial β oxidation of exogenous FFAs or other lipids to support both their longevity and protective function. Although T_{CM} cells depend in part on fatty-acid oxidation for cellular metabolism[17,28], our data show that T_{CM} cells cannot

effectively internalize exogenous FFAs. Cell-intrinsic lipolysis and increased glycerol transport are used by T_{CM} cells to support metabolic programming necessary for development[17,28,29], but the dependence upon exogenous FFA uptake and metabolism for long-term survival is unique to T_{RM} cells. Additionally, it is noteworthy that similar results were obtained from mice injected intradermally with etomoxir and mice with *Cpt1a* knockdown in OT-I cells (Fig. 2g and Extended Data Fig. 8a, b), suggesting that the etomoxir effects on $CD8^+$ T_{RM} cell persistence were mediated through CPT1A[30]. Given that generation of long-lived T_{RM} cells are a goal of effective vaccination[4], and that dysfunction of T_{RM} cells underlies many auto-inflammatory tissue disorders[4,5], a more detailed understanding of the unique lipid metabolic programs intrinsic to T_{RM} cells and how these programs might be manipulated to increase or decrease T_{RM} cell longevity and function, will be a subject of future investigation.

METHODS

Mice

Wide-type C57BL/6, $CD45.1^+$, $Thy1.1^+$, $Rag1^{-/-}$ and μMT mice were purchased from Jackson Laboratory. $Thy1.1^+$ $Rag1^{-/-}$ OT-I mice were maintained through routine breeding in the animal facility of Harvard Institute of Medicine, Harvard Medical School. *Fabp4*$^{-/-}$, *Fabp5*$^{-/-}$, and *Fabp4*$^{-/-}$/*Fabp5*$^{-/-}$ mice were provided by G.S.H. Mice were bred to generate $Thy1.1^+$ $CD45.1^+$ wild-type; $Thy1.1^+$ $CD45.2^+$ *Fabp4*$^{-/-}$/*Fabp5*$^{-/-}$; $Thy1.1^+$ $CD45.1^+$ wild-type OT-I, $Thy1.1^+$ $CD45.2^+$ *Fabp4*$^{+/-}$*Fabp5*$^{+/-}$ OT-I, $Thy1.1^+$ $CD45.2^+$ *Fabp4*$^{-/-}$ OT-I, $Thy1.1^+$ $CD45.2^+$ *Fabp5*$^{-/-}$ OT-I and $Thy1.1^+$ $CD45.2^+$ *Fabp4*$^{-/-}$/*Fabp5*$^{-/-}$ OT-I mice. Animal experiments were performed in accordance with the guidelines put forth by the Center for Animal Resources and Comparative Medicine at Harvard Medical School, and all protocols and experimental plans were approved by the HMS IACUC beforehand. Mice were randomly assigned to each group before the start and experiments were performed blinded with respect to treatment. For survival experiments, mice that had lost over 25% of their original body weight were euthanized.

Viruses and infections

Recombinant VACV expressing the OT-I T cell epitope $OVA_{257–264}$ and Western Reserve strain (WR-VACV) were originally obtained from B. Moss (NIH). Virus was expanded and titred by standard procedures as described previously[9]. 2×10^6 p.f.u. of $VACV_{OVA}$ was used for infection by either skin scarification or intratracheal infection. 2×10^6 p.f.u. WR-VACV was used at a lethal dose for intranasal infections, as described previously[9].

Antibodies and flow cytometry

The following anti-mouse antibodies were obtained from BD PharMingen: PerCP-conjugated anti-CD3e (553067), PE-conjugated anti-CD8 (557654), PE-Cy7-conjugated anti-CD8 (552877), APC-Cy7-conjugated anti-CD8 (557654), PE-conjugated anti-Thy1.1 (561404), APC-conjugated anti-Thy1.1 (557266), Alexa Fluor 488-conjugated anti-KLRG1 (561619), PE-conjugated anti-integrin α4β7 (553811), PE-Cy7-conjugated anti-CD62L (560516), APC-Cy7-conjugated CD62L (560514), APC-conjugated anti-IFNγ (554413). Anti-mouse antibodies were also obtained from Biolegend: Alexa Fluor 488-conjugated

anti-CD3e (100321), Alexa Fluor 647-conjugated anti-CD4 (100424), Alexa Fluor 594-conjugated anti-Ep-CAM (118222), FITC-conjugated anti-CD45.1 (110706), PE-conjugated anti-CD45.1 (110708), PE-Cy7-conjugated anti-CD45.2 (109830), APC-conjugated anti-CD45.2 (109814), PE-conjugated anti-CD45.2 (109808), APC-conjugated anti-KLRG1 (138412), PE-conjugated anti-CD44 (103008), PE-Cy7-conjugated anti-CD44 (103030), PE-Cy7-conjugated anti-CD69 (104512), APC-conjugated anti-CD103 (121414), APC-conjugated anti-integrin α4β7 (120608). The following anti-human antibodies were obtained from Biolegend: APC-Cy7-conjugated anti-CD3 (300425), PerCp-conjugated anti-CD4 (317431), APC-conjugated anti-CD8 (300911), Alexa Fluor 488-conjugated anti-CD69 (310916), PE-Cy7-conjugated anti-CD69 (310911), PE-conjugated anti-CD62L (304805), FITC-conjugated anti-CD45RO (304204). Antibodies were also obtained from Abcam: anti-human FABP4 (9B8D) and NOVUS: Alexa Fluor 405-conjugated anti-human FABP5 (FAB3077V). PE-conjugated B8R20–27/H-2Kb pentamers were obtained from ProImmune Ltd, and stained according to the manufacturer's protocol. E- or P-selectin ligand expression was analysed by incubating cells with rmE-Selectin/Fc Chimera (575-ES; R&D System) or rmP-Selectin/Fc Chimera (737-PS; R&D System) in conjunction with PerCP-conjugated F(ab')2 fragments of goat anti-human IgG F(c) antibody (109-126-170; Jackson ImmunoResearch). To measure *ex vivo* uptake of Bodipy-conjugated palmitate (Bodipy FL C_{16}; D-3821; Thermo Fisher), cells were incubated for 30 min at 37 °C with 1 μM Bodipy FL C_{16} in PBS with 20 μM FA-free BSA (A8806; Sigma-Aldrich). Bodipy uptake was quenched by adding 4× volume of ice-cold PBS with 2% FBS and then cells were washed twice before flow cytometry analysis. Annexin V staining was included to exclude dead/dying cells during FACS data acquisition. To block Bodipy uptake, cells were incubated with 100 μM palmitic acid (P0500; Sigma-Aldrich) for 10 min at 37 °C before Bodipy addition. Apoptosis was measured with the FITC Annexin V Apoptosis Detection Kit (640922; Biolegend) according to the manufacturer's protocol. Flow cytometry data were acquired with a FACS Canto II flow cytometer (BD Biosciences) and data were analysed with Flowjo software (Tree Star).

Preparation of cell suspensions

Lymph nodes and spleen were collected and pressed through a 70-μm nylon cell strainer to prepare cell suspensions. Red blood cells (RBC) were lysed using RBC lysis buffer (00-4333-57; eBioscience). Skin tissue was excised after hair removal, separated into dorsal and ventral halves, minced, and then incubated in Hanks balanced salt solution (HBSS) supplemented with 1 mg ml^{-1} collagenase A (11088785103; Roche) and 40 μg ml^{-1} DNase I (10104159001; Roche) at 37 °C for 30 min. After filtration through a 70-μm nylon cell strainer, cells were collected and washed three times with cold PBS before staining.

Mouse adoptive transfer and treatment

Lymph nodes were collected from naive female donor mice at the age of 6–8 weeks. T cells were purified by magnetic cell sorting using a mouse $CD8\alpha^+$ T-cell isolation kit (130-104-075; Miltenyi Biotec) or a mouse $CD4^+$ T-cell isolation kit (130-104-454; Miltenyi Biotec), according to the manufacturer's protocols. T cells were then transferred intravenously into female recipient mice at a total number of 5×10^5 or 2.5×10^5 cells per population in co-transfer experiments where cell types were transferred at a ratio of 1:1. To

generate mixed bone-marrow chimaeras, T-cells- and NK-cell-depleted Thy1.1$^+$ CD45.1$^+$ wild-type and Thy1.1$^+$ CD45.2$^+$ *Fabp4*$^{-/-}$/*Fabp5*$^{-/-}$ bone marrow was mixed in a 1:1 ratio and transferred at a number of 1×10^6 cells per population into sublethally irradiated recipient mice. Mice were rested for eight weeks before infection for full reconstitution of T cells and restoration of an intact immune system. Rag1$^{-/-}$ T-cell reconstituted mice were generated by adoptive transfer of 3.5×10^6 CD4$^+$ cells with 2×10^6 CD8$^+$ wild-type or CD8$^+$ *Fabp4*$^{-/-}$/*Fabp5*$^{-/-}$ cells. T cells were labelled with carboxyfluorescein succinimidyl ester (CFSE, 65-0850; eBioscience) before co-transfer, where indicated. In some experiments, mice were treated daily with FTY720 (10006292; CAYMAN, 1 mg per kg) by intraperitoneal injection or with etomoxir (E1905; Sigma-Aldrich, 1 μg per site), GW9662 (M6191, Sigma-Aldrich, 1 mg per kg) or trimetazidine (653322, Sigma-Aldrich, 1 mg per kg) by intradermal injection.

Microarray, data analysis and qPCR

For each microarray dataset, OT-I cells from 15–20 mice were sorted with a FACSAria III (BD Biosciences) and pooled. RNA was extracted with an RNeasy Micro kit (74004; Qiagen). RNA quality and quantity was assessed with a Bioanalyzer 2100 (Agilent). RNA was then amplified and converted into cDNA by a linear amplification method with a WT-Ovation Pico System (3302-60; Nugen). Subsequently cDNA was labelled with the Encore Biotin module (4200-60; Nugen) and hybridized to GeneChip MouseGene 2.0 ST chips (Affymetrix) at the Translational Genomics Core of Partners Healthcare, Harvard Medical School. GeneChips were scanned using the Affymetrix GeneChip Scanner 3000 7G running Affymetrix Gene Command Console version 3.2. The data were analysed by using the Affymetrix Expression Console version 1.3.0.187 using the analysis algorithm RMA. To evaluate overall performance of microarray data, principal-component analysis and Pearson correlation coefficients among 12 diverse samples were applied by using 26,662 transcripts (R program).

For relative qPCR, RNA was prepared as described above. A Bio-Rad iCycler iQ Real-Time PCR Detection System (Bio-Rad) was used with the following settings: 45 cycles of 15 s of denaturation at 95 °C, and 1 min of primer annealing and elongation at 60 °C. qPCR was performed with 1 μl cDNA plus 12.5 μl of 2× iQ SYBR Green Supermix (Bio-Rad) and 0.5 μl (10 μM) specific primers: mouse *Fabp4* forward (5′-TTTCCTTCAAACTGGGCGTG-3′) and mouse *Fabp4* reverse (5′-CATTCCACCACCAGCTTGTC-3′); mouse *Fabp5* forward (5′-AACCGAGAGCACAGTGAAG-3′) and mouse *Fabp5* reverse (5′-ACACTCCACGATCATCTTCC-3′); mouse *Pparg* forward (5′-TCGCTGATGCACTGCCTATG-3′) and mouse *Pparg* reverse (5′-GAGAGGTCCACAGAGCTG ATT-3′); mouse *Actb* forward (5′-CATTGCTGACAGGATGCAGAAGG-3′) and mouse *Actb* reverse (5′-TGCTGGAAGGTGGACAGTGAGG-3′). For absolute qPCR, each standard curve was constructed using tenfold serial dilutions of the target gene template ranging from 10^7 to 10^2 copies per ml and obtained by plotting values of the logarithm of their initial template copy numbers versus the mean C_t values. The actual copy numbers of target genes were determine by relating the C_t value to a standard curve.

Immunofluorescence microscopy

Mice were perfused with buffer A (0.2 M NaH_2PO_4, 0.2 M Na_2HPO_4, 0.2 M L-lysine and 0.1 M sodium periodate with 2% paraformaldehyde) and infected skin sites were collected and incubated for 30 min on ice in buffer A. Skin tissue was washed twice with PBS and incubated for 30 min at 4 °C in 20% sucrose. Fixed tissue was embedded in OCT (Tissue Tek IA018; Sakura) and frozen in liquid nitrogen. Skin sections were performed on a cryostat (Leica CM1850 UV) at 6-μm thickness and air-dried for 6–8 h. Sections were then fixed in −20 °C acetone for 5 min, rehydrated with PBS, and blocked with 2% FCS in PBS for 15 min at room temperature (20 °C). Sections were stained with rabbit anti-mouse/human FABP4 antibody (EPR3579; ab92501, Abcam), rabbit anti-mouse/human FABP5 (H-45, sc-50379, Santa Cruz) overnight at 4 °C in a semi-humid chamber. Sections were rinsed for 10 min in PBS, and labelled with donkey anti-rabbit Rhodamine Red-X (711-296-152; Jackson ImmunoResearch) for 1 h at room temperature (20 °C). Sections were rinsed for 10 min in PBS, and stained with Alexa Fluor 647-conjugated anti-mouse Thy1.1 (202508, Biolegend) in PBS for 1 h at room temperature. Then sections were rinsed three times (for 5 min each time) with TBS-Tween 20 by shaking and mounted with ProLong Diamond Antifade Mountant with DAPI (P36962; ThermoFisher). For tissue lipid visualization, sections were stained with BODIPY 493/503 (4,4-Difluoro-1,3,5,7,8-Pentamethyl-4-Bora-3a,4a-Diaza-s-Indacene) (D3922, Molecular Probes) before being mounted. Images were acquired with a Leica TCS SP8 confocal microscope (Harvard NeuroDiscovery Center Optical Imaging Core) and analysed with ImageJ.

Lentiviral siRNA transduction

Scrambled, *Pparg* and *Cpt1a* siRNA GFP lentiviruses were purchased from ABM (Applied Biological Materials Inc.) with sequences as follows. Scrambled siRNA: GGGTGAACTCACGTCAGAA; *Pparg* KD1: AATATGACCTGAAGCTCCAAGAATA; *Pparg* KD2: GTCTGCTGATCTGCGAGCC; *Cpt1a* KD1: GGAGCGACTCTTCAATACTTCCCGCATCC, *Cpt1a* KD2: GGTCATAGAGACATCCCTAAGCAGTGCCA.

For siRNA lentivirus transduction, OT-I mice were infected with 2×10^6 $VACV_{OVA}$ by skin scarification. After 60 h, $CD8^+$ T cells were collected from draining lymph nodes and incubated in medium with 10 μg ml^{-1} polybrene and 20 ng ml^{-1} hIL-2 at 37 °C for 30 min. Then cells were infected with scrambled, *Pparg* or *Cpt1a* siRNA GFP lentiviruses, in the presence of ViralPlus Transduction Enhancer G698 at 1:100 in order to enhance transduction efficiency. For adoptive transfer, 2.5×10^5 *Pparg* or *Cpt1a* siRNA transduced OT-I cells (together with the same number of congenically scrambled-siRNA-transduced OT-I cells) were co-transferred into recipient mice that were previously infected with 2×10^6 $VACV_{OVA}$ by skin scarification. After 40 days, mice were euthanized and the number of siRNA-transduced OT-I cells in the infected skin tissue were isolated and enumerated by flow cytometry on the basis of the GFP marker. Recipient and both donor populations used for co-transfers differed in CD90 and CD45 alleles (CD90.2/45.2, CD90.1/45.1 or CD90.1/45.2—the combinations differed between experiments) to allow for identification of donor populations.

Fatty-acid oxidation assay

Oxidation of exogenous FFAs was measured using the XF Palmitate-BSA FAO substrate with the XF cell mito stress kit according to the manufacturer's protocol (Seahorse Bioscience). Freshly isolated and sorted T cells (2.5×10^5) were incubated for 30 min with fatty-acid oxidation assay medium (111 mM NaCl, 4.7 mM KCl, 1.25 mM $CaCl_2$, 2.0 mM $MgSO_4$, 1.2 mM Na_2HPO_4, 2.5 mM glucose, 0.5 mM carnitine and 5 mM HEPES). When required, cells were pre-treated with etomoxir (40 μM) for 15 min. Afterwards, BSA (34 μM) or palmitate-BSA (200 μM palmitate conjugated with 34 μM BSA) was added to the medium, and the OCR was measured under basal conditions and in response to 1 μM oligomycin, 1.5 μM fluorocarbonyl cyanide phenylhydrazone (FCCP), and 100 nM rotenone + 1 μM antimycin A. Results were normalized to data from control cells in the presence of BSA.

Determination of viral load

VACV load was evaluated by qPCR as described previously[3]. In brief, 6 days after re-infection, inoculated skin samples were collected and DNA was purified with the DNeasy Mini Kit (51304; Qiagen) according to the manufacturer's protocol. qPCR was performed with the Bio-Rad iCycler iQ Real-Time PCR Detection System (Bio-Rad Laboratories). The primers and TaqMan probe used in the qPCR assay are specific for the ribonucleotide reductase Vvl4L of VACV. The sequences are (forward) 5′-GACACTCTGGCAGCCGAAAT-3′; (reverse) 5′-CTGGCGGCTAGAATG GCATA-3′; (probe) 5′-AGCAGCCACTTGTACTACACAACATCCGGA-3′. The probe was 5′-labelled with FAM and 3′-labelled with TAMRA (Applied Biosystems). Amplification reactions were performed in a 96-well PCR plate (Bio-Rad Laboratory) in a 20 μl volume containing 2× TaqMan Master Mix (Applied Biosystems), 500 nM forward primer, 500 nM reverse primer, 150 nM probe, and the template DNA. Thermal cycling conditions were 50 °C for 2 min and 95 °C for 10 min for 1 cycle, followed by 45 cycles of amplification (94 °C for 15 s and 60 °C for 1 min). To calculate the viral load, a standard curve was generated from DNA of a VACV stock with a previously determined titre. Corresponding C_t values obtained by the qPCR methods were plotted on the standard curve to estimate viral load in the skin samples.

Intracellular cytokine detection

Infected skin was collected 6 days after $VACV_{OVA}$ re-infection and single-cell suspensions were prepared as described above. Cells were then incubated with 2 μg ml^{-1} SINFEKL peptide of ovalbumin (RP 10611; GenScript) in the presence of brefeldin A (00-4506-51; eBioscience) for 7 h. Fc receptors were blocked with CD16/CD32 monoclonal antibodies (14-0161-82; eBioscience). Subsequently, intracellular IFNγ (554413; BD) as well as IFNγ isotype control (554686; BD) staining was performed using Intracellular Cytokine Detection Kits (BD Bioscience) according to the manufacturer's instructions before data acquisition on a flow cytometer.

Human tissue samples

This is an experimental laboratory study performed on human tissue samples. All studies were performed in accordance with the Declaration of Helsinki. Blood from healthy individuals was obtained after leukapheresis, and normal skin was obtained from healthy individuals undergoing cosmetic surgery procedures. Lesional skin from patients with psoriasis was obtained from patients seen at the Brigham and Women's Hospital or at Rockefeller University. All tissues were collected with informed consent (where applicable) and with prior approval from the Partners or Rockefeller Institutional Review Boards. Skin tissue was extensively minced and then incubated for 2 h at 37 °C in RPMI-1640 containing 0.2% collagenase type I (Invitrogen) and 30 Kunitz units per ml DNase I (Sigma Aldrich). Subsequently, cells were collected by filtering the collagenase-treated tissue through a 40-μm cell strainer (Fisher Scientific) followed by two washes with culture medium to remove any residual enzyme. Cells were stained with directly conjugated antibodies and analysed by flow cytometry. Gate strategy: T_N cells, $CD45RA^+CD45RO^-CD3^+CD8^+CD62L^+$; T_{CM} cells, $CD45RO^+CD3^+CD8^+CD62L^+CCR7^+$; T_{EM} cells, $CD45RO^+CD3^+CD8^+CD62L^-CCR7^-$; T_{RM} cells, $CD45RO^+CD3^+CD8^+CD62L^-CD69^+$. For immunofluorescent staining, skin tissues were embedded in OCT and frozen in liquid nitrogen immediately after surgery.

Statistical analysis

Comparisons between two groups were calculated using Student's *t*-test (two tailed). Comparisons between more than two groups were calculated with one-way analysis of variance (ANOVA) followed by Bonferroni's multiple comparison tests. Two-way ANOVA with Holm–Bonferroni post hoc analysis was used to compare weight loss between groups and log-rank (Mantel–Cox) test was used for survival curves. $P < 0.05$ was considered statistically significant.

Data availability

The microarray data that support the findings of this study are available in the Gene Expression Omnibus (accession number GSE79805); and Source Data are provided with the paper.

Extended Data

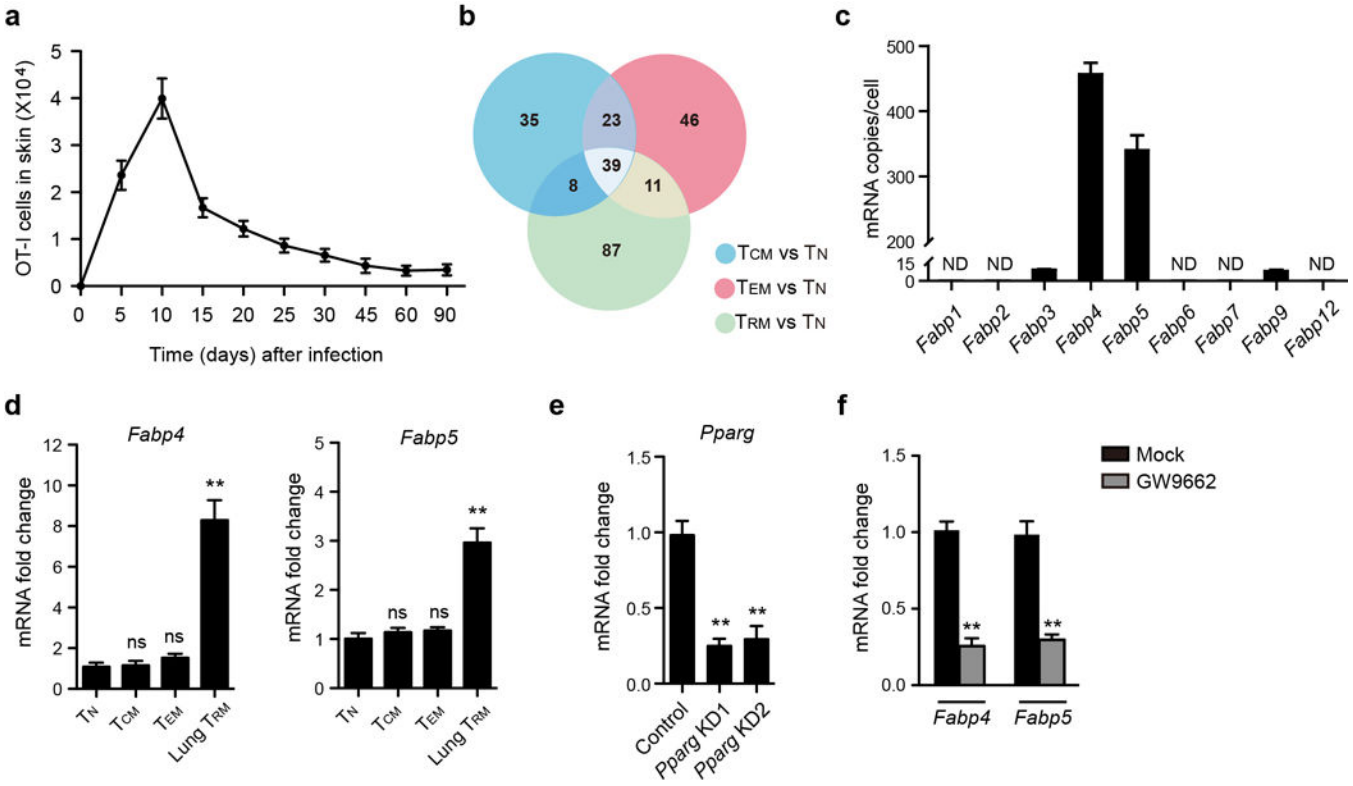

Extended Data Figure 1. CD8$^+$ T_{RM} cells show increased gene expression of *Fabp4* and *Fabp5*

a, Number of OT-I Thy1.1$^+$ cells in infected skin at indicated time after infection. Graph shows mean ± s.d. of 10 mice. **b**, Venn diagram analysis of genes differentially expressed in pairwise comparisons between OT-I T_{CM}, T_{EM} and T_{RM} cells (day 30) relative to that of T_N cells (fold change cutoff, ≥ 2). **c**, Absolute qPCR analysis of *Fabp* gene expression in T_{RM} cells (day 30). ND, not detectable. **d**, qPCR assessments of *Fabp4* and *Fabp5* levels in indicated T cell subsets. OT-I Thy1.1$^+$ cells were intravenously transferred into Thy1.2$^+$ recipient mice 1 day before mice were infected with 2×10^6 p.f.u. $VACV_{OVA}$ by intratracheal infection. After 45 days, mice were euthanized. T_{CM} and T_{EM} cells were sorted from spleen and T_{RM} cells were sorted from lung. **e**, qPCR analysis of *Pparg*-knockdown efficiency by lentiviral vector encoding two specific and one scrambled siRNA in OT-I CD8$^+$ T_{RM} cells. **f**, qPCR analysis of *Fabp4* and *Fabp5* gene expression in OT-I CD8$^+$ T_{RM} cells from mice treated with or without GW9662. Graphs in **c**, **d**, **e**, **f** show mean ± s.d. from triplicates. β-actin was used as internal control and mRNA was normalized to T_N samples (**d**), or T_{RM} samples with scrambled siRNA transduction (**e**) or without GW9662 treatment (**f**). T cells from 15–20 mice were pooled for each sample. $^{**}P < 0.01$; NS, not significant.

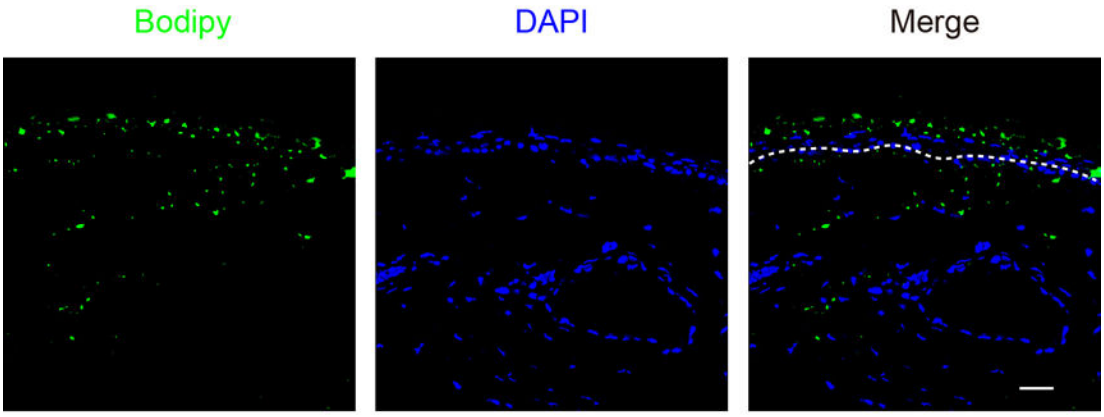

Extended Data Figure 2. Visualization of lipid distribution in mouse skin tissue by Bodipy staining

Mouse skin cryosections were stained for lipids (4,4-Difluoro-1,3,5,7,8-Pentamethyl-4-Bora-3a,4a-Diaza-s-Indacene (BODIPY 493/503), green) and nuclei (4′,6-diamidino-2-phenylindole (DAPI), blue). Images were acquired with a Leica TCS SP8 confocal microscope and analysed with ImageJ. $n = 15$ sections from 5 mice and 1 representative site is shown. Dashed line indicates epidermal–dermal boundary. Scale bar, 20 μm.

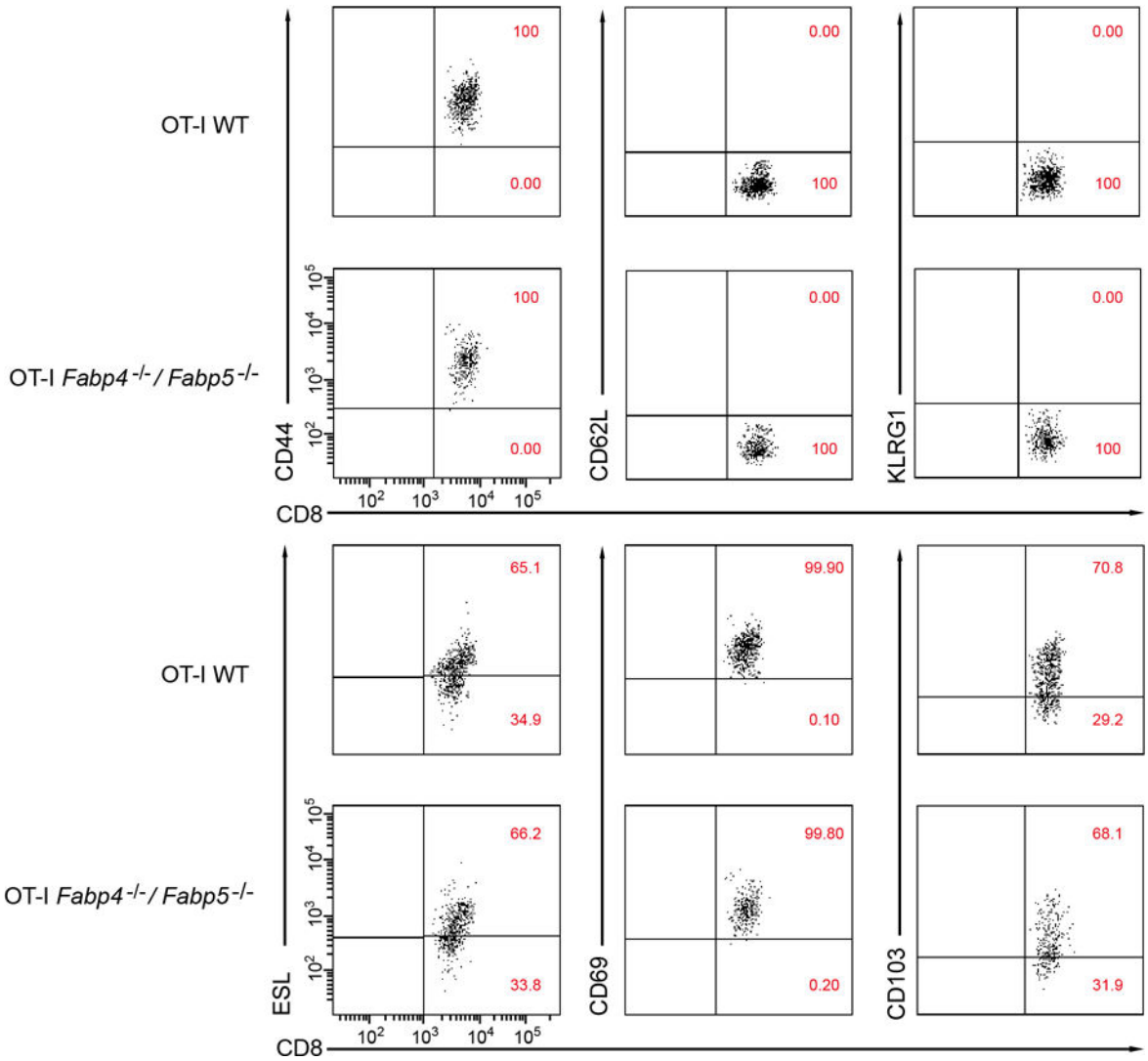

Extended Data Figure 3. OT-I *Fabp4*$^{-/-}$/*Fabp5*$^{-/-}$ T_{RM} cells show a similar surface protein expression phenotype as wild-type cells

Thy1.2$^+$ CD45.2$^+$ recipient mice were given a 1:1 ratio of naive OT-I Thy1.1$^+$ CD45.1$^+$ wild-type and OT-I Thy1.1$^+$ CD45.2$^+$ *Fabp4*$^{-/-}$/*Fabp5*$^{-/-}$ cells one day before mice were infected with 2×10^6 p.f.u. $VACV_{OVA}$ by skin scarification. Subsequently, 45 days after infection, infected skin sites were collected and the phenotype of T_{RM} cells was examined by flow cytometry. Data are representative of three independent experiments ($n = 5$ mice per group). ESL, E-selectin ligand.

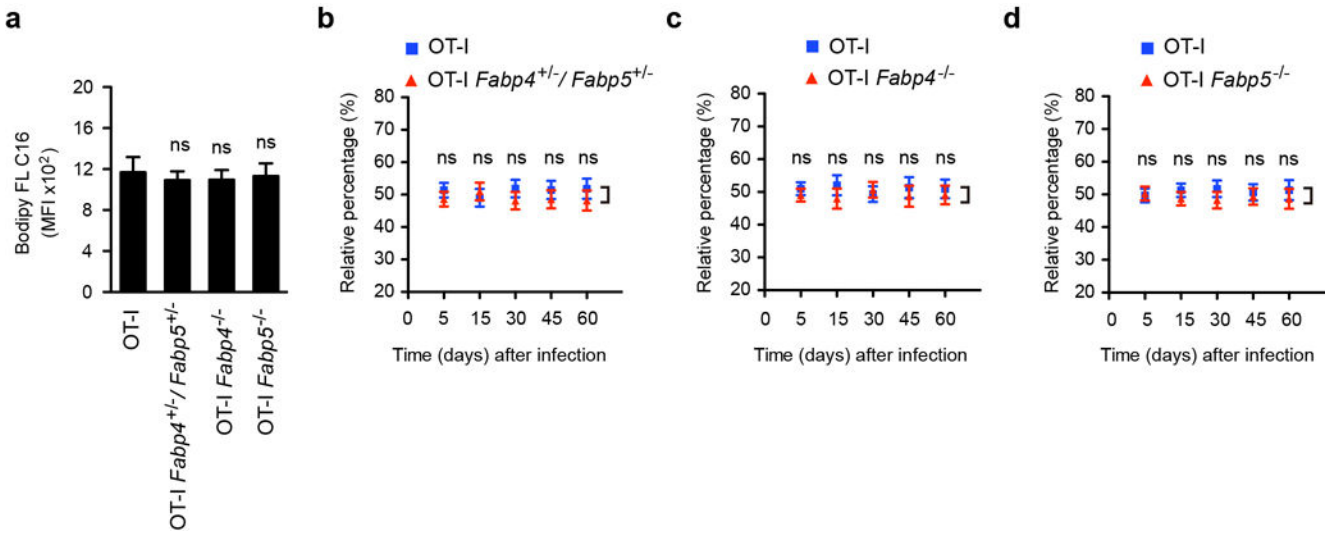

Extended Data Figure 4. Relative contribution of FABP4 and FABP5 in fatty acid acquisition and long-term maintenance of skin CD8$^+$ T_{RM} cells

a, Average MFI of Bodipy FL C_{16} uptake by OT-I wild-type, *Fabp4*$^{+/-}$*Fabp5*$^{+/-}$, *Fabp4*$^{-/-}$ and *Fabp5*$^{-/-}$ T_{RM} cells. **b**–**d**, Number of OT-I wild-type, *Fabp4*$^{+/-}$*Fabp5*$^{+/-}$, *Fabp4*$^{-/-}$ and *Fabp5*$^{-/-}$ T_{RM} cells at different time points after $VACV_{OVA}$ infection. Thy1.2$^+$ CD45.2$^+$ recipient mice were given a 1:1 ratio of naive OT-I Thy1.1$^+$ CD45.1$^+$ wild-type and OT-I Thy1.1$^+$ CD45.2$^+$ *Fabp4*/*Fabp5* knockout cells (*Fabp4*$^{+/-}$*Fabp5*$^{+/-}$ (**b**), *Fabp4*$^{-/-}$ (**c**) or *Fabp5*$^{-/-}$ (**d**) cells) one day before infection with 2×10^6 p.f.u. $VACV_{OVA}$ by skin scarification. Relative percentages of the two T cell populations were analysed longitudinally by flow cytometry. Graphs show mean ± s.d. of 5 mice per group. NS, not significant.

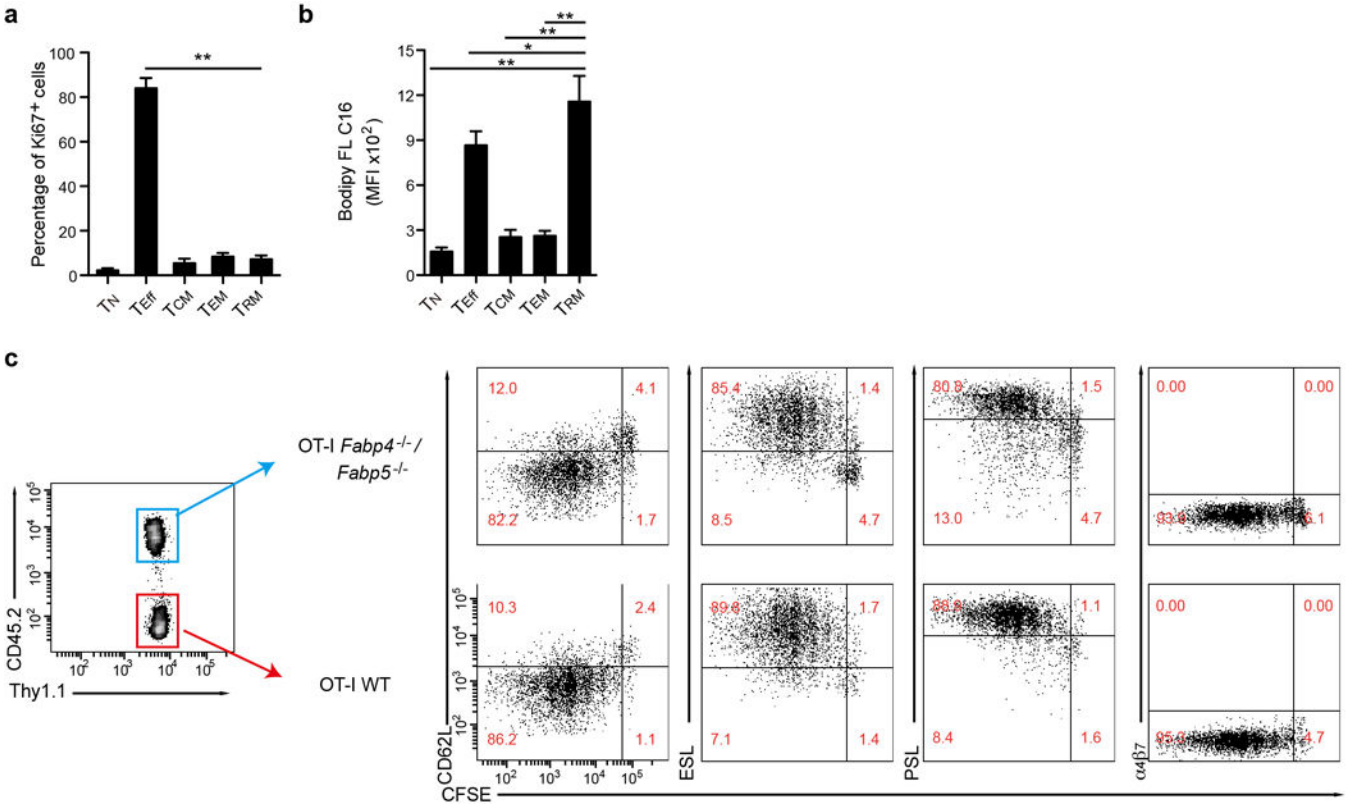

Extended Data Figure 5. OT-I *Fabp4*$^{-/-}$/*Fabp5*$^{-/-}$ T_{eff} cells have similar proliferative capacity and tissue-homing receptor expression as wild-type counterparts

a, Quantification of Ki67$^+$ cells in OT-I T_N, T_{eff}, T_{CM}, T_{EM} and T_{RM} cells. **b**, Average MFI of Bodipy FL C_{16} uptake by OT-I T_N, T_{eff}, T_{CM}, T_{EM} or T_{RM} cells. Graphs show mean ± s.d. of 5 mice per group (**a**, **b**). *$P < 0.05$; **$P < 0.01$. **c**, Flow cytometric analysis of T cell proliferation and homing receptor expression on OT-I wild-type and *Fabp4*$^{-/-}$/*Fabp5*$^{-/-}$ T cells. Thy1.2$^+$ CD45.2$^+$ recipient mice were given a 1:1 ratio of CFSE-labelled naive OT-I Thy1.1$^+$ CD45.1$^+$ wild-type and OT-I Thy1.1$^+$ CD45.2$^+$ *Fabp4*$^{-/-}$/*Fabp5*$^{-/-}$ cells one day before mice were infected with 2×10^6 p.f.u. $VACV_{OVA}$ by skin scarification. At 60 h after infection, proliferation and tissue-homing receptor expression of OT-I cells isolated from draining lymph nodes were analysed by flow cytometry. Data are representative of three independent experiments ($n = 5$ mice per group). ESL, E-selectin ligand; PSL, P-selectin ligand.

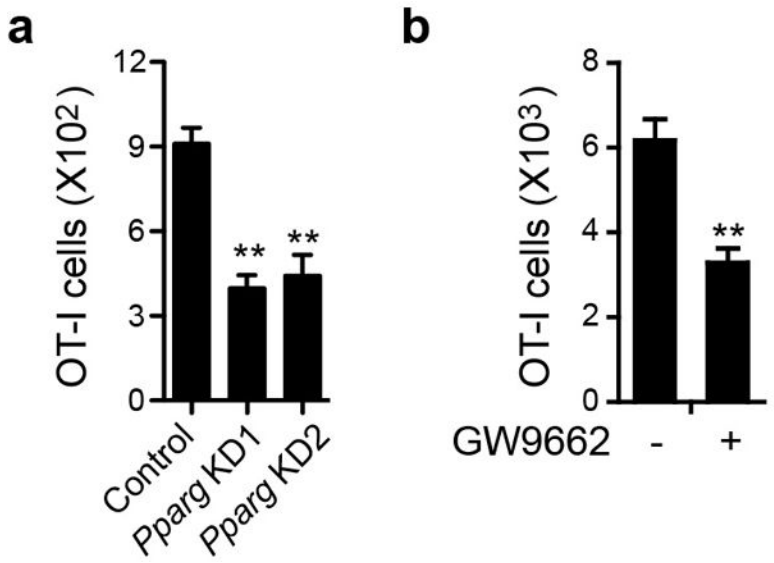

Extended Data Figure 6. Effect of *Pparg* lentiviral siRNA knockdown or PPARγ inhibition on CD8$^+$ T$_{RM}$ cell maintenance in peripheral tissue

a, Number of OT-I CD8$^+$ T$_{RM}$ transduced with scrambled siRNA or siRNA targeting *Pparg*. OT-I cells transduced with *Pparg* siRNA (together with the same number of congenically scrambled siRNA transduced OT-I cells) were cotransferred into recipient mice that were previously infected with VACV$_{OVA}$ by skin scarification. After 40 days, mice were euthanized and the number of siRNA-transduced OT-I cells in the infected skin tissue were collected and counted by flow cytometry on the basis of the GFP marker. **b**, Number of OT-I CD8$^+$ T$_{RM}$ cells in infected skin from mice treated with or without GW9662. Thy1.2$^+$ CD45.2$^+$ recipient mice were infected with 2×10^6 p.f.u. VACV$_{OVA}$ by skin scarification. 40 days later, mice were treated with GW9662 daily by intradermal injection for 5 days, after which mice were euthanized and T$_{RM}$ cells were counted and analysed by flow cytometry. Graphs show mean ± s.d. of 5 mice per group. $^{**}P < 0.01$.

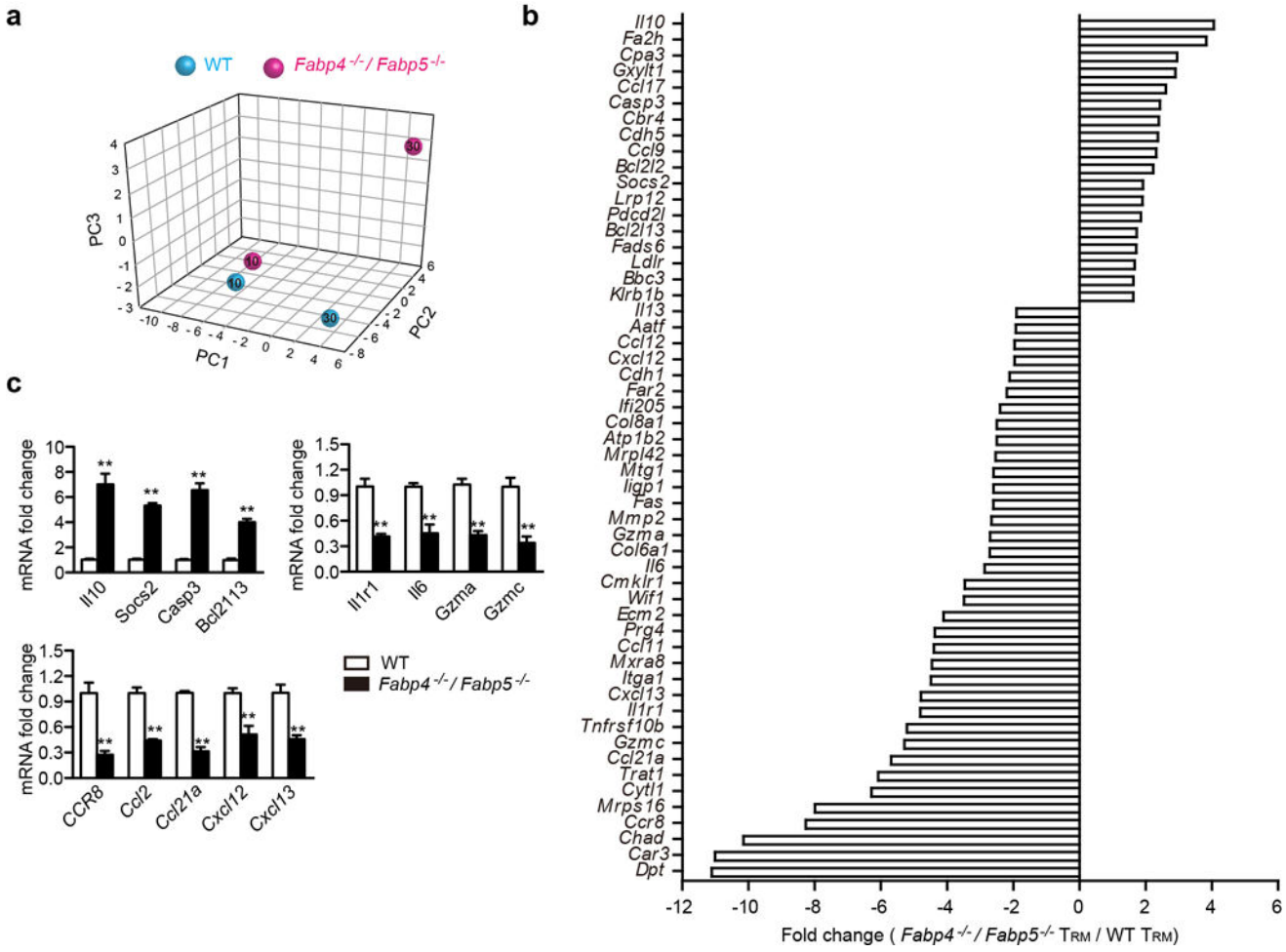

Extended Data Figure 7. Gene expression profile of OT-I *Fabp4*$^{-/-}$/*Fabp5*$^{-/-}$ T_{RM} cells

a, Principal-component analysis of gene-expression data for skin infiltrating T cells isolated at day 10 and day 30 after infection. **b**, Differentially expressed genes selected from a pairwise comparison between OT-I *Fabp4*$^{-/-}$/*Fabp5*$^{-/-}$ T_{RM} and OT-I wild-type T_{RM} cells. Thy1.2$^+$ CD45.2$^+$ recipient mice were given a 1:1 ratio of naive OT-I Thy1.1$^+$ CD45.1$^+$ wild-type and OT-I Thy1.1$^+$ CD45.2$^+$ *Fabp4*$^{-/-}$/*Fabp5*$^{-/-}$ cells one day before mice were infected with 2×10^6 p.f.u. $VACV_{OVA}$ by skin scarification. At 30 days after infection, OT-I CD8$^+$ T_{RM} cells were sorted from infected skin sites for gene microarray. **c**, qPCR analysis of genes involved in anti-inflammatory responses (*Il10* and *Socs2*), cell apoptosis (*Casp3* and *Bcl2113*) as well as immune responses (*Ccr8*, *Ccl21*, *Il1r1*, *Il6*, *Cxcl13*, *Cxcl12*, *Ccl12*, *Gzmc*, *Gzma*) in OT-I *Fabp4*$^{-/-}$/*Fabp5*$^{-/-}$ T_{RM} cells compared to wild-type T_{RM} cells. Graphs show mean ± s. d. from triplicates. β-actin was used as internal control and mRNA was normalized to OT-I wild-type T_{RM} cells. mRNA was pooled from 15 mice from 3 independent biological groups (5 mice per group). $^{**}P < 0.01$.

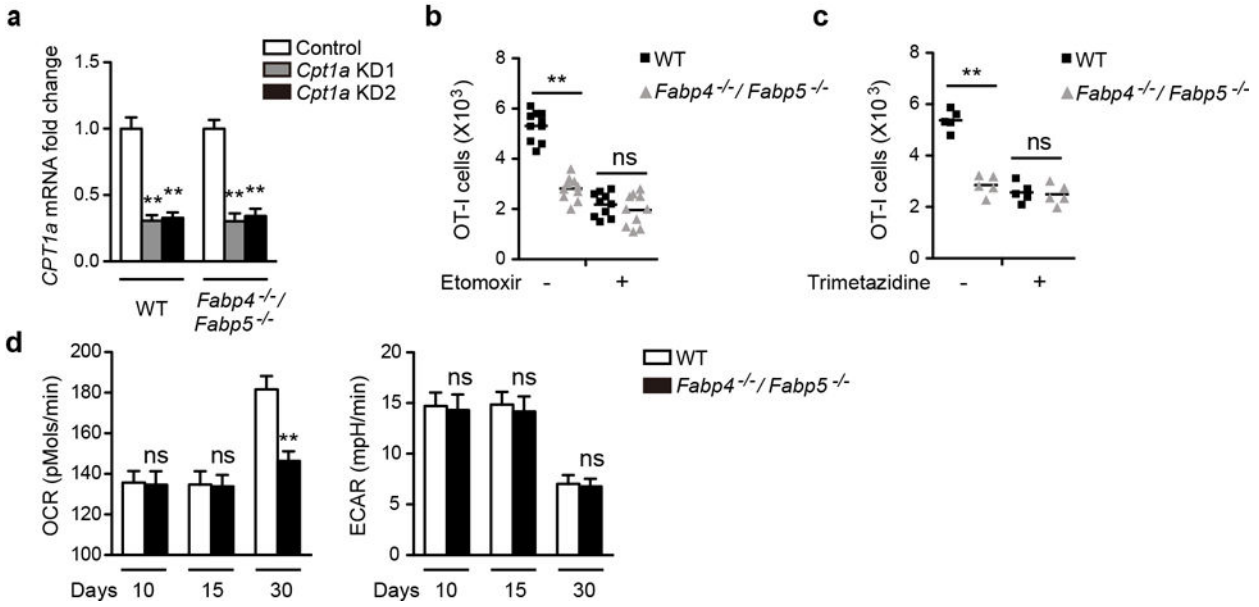

Extended Data Figure 8. Effect of *Cpt1a* lentiviral siRNA knockdown or CPT1A inhibition on OT-I CD8$^+$ T_{RM} cell maintenance in peripheral tissue

a, qPCR analysis of *Cpt1a* lentiviral siRNA knockdown efficiency in OT-I CD8$^+$ T_{RM} cells. **b**, **c**, Quantification of OT-I wild-type and OT-I *Fabp4*$^{-/-}$/*Fabp5*$^{-/-}$ T_{RM} cells in infected skin from mice treated with or without etomoxir (**b**) or trimetazidine (**c**). Thy1.2$^+$ CD45.2$^+$ recipient mice were given a 1:1 ratio of naive OT-I Thy1.1$^+$ CD45.1$^+$ wild-type and OT-I Thy1.1$^+$ CD45.2$^+$ *Fabp4*$^{-/-}$/*Fabp5*$^{-/-}$ cells one day before infection with 2 × 10^6 p.f.u. $VACV_{OVA}$ by skin scarification. Mice were administered etomoxir or trimetazidine daily by intradermal injection for 5 days from day 40 after infection, after which mice were euthanized and T_{RM} cells were analysed by flow cytometry and counted. Symbols represent individual mice. **d**, OCR and ECAR as measured by the Seahorse assay of skin-infiltrating T cells sorted at indicated time points after infection under basal conditions. Graphs show mean ± s.d. of triplicates. $^{**}P < 0.01$; NS, not significant.

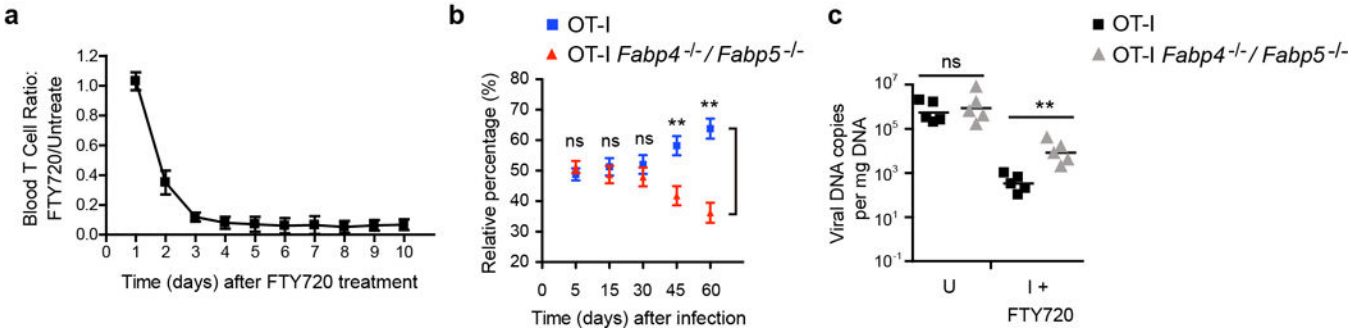

Extended Data Figure 9. Skin CD8$^+$ T_{RM} cells residing in distal infection sites are deficient in long-time survival and virus clearance

a, Ratio of peripheral blood CD3 counts in FTY720 versus untreated mice, illustrating the kinetics of lymphoid sequestration by FTY720. $n = 5$ mice per group. **b**, Quantification of OT-I wild-type and OT-I *Fabp4*$^{-/-}$/*Fabp5*$^{-/-}$ cells infiltrating distal infection sites at different

time points after $VACV_{OVA}$ infection. Thy1.2$^+$ CD45.2$^+$ recipient mice were given a 1:1 ratio of naive OT-I Thy1.1$^+$ CD45.1$^+$ wild-type and OT-I Thy1.1$^+$ CD45.2$^+$ *Fabp4*$^{-/-}$/*Fabp5*$^{-/-}$ cells one day before infection with 2×10^6 p.f.u. $VACV_{OVA}$ by skin scarification of the right ears. Relative percentages of the two T cell populations infiltrating left ears were analysed longitudinally by flow cytometry. Graphs show mean ± s.d. of 5 mice per group. **c**, qPCR analysis of distal infection skin viral load at six days after re-challenge. OT-I wild-type or OT-I *Fabp4*$^{-/-}$/*Fabp5*$^{-/-}$ cells were adoptively transferred into μMT mice before infection with 2×10^6 p.f.u. $VACV_{OVA}$ by skin scarification of the right ears. 25 days later, mice were re-challenged with $VACV_{OVA}$ at the left ear by skin scarification. U, unimmunized; I, immunized mice. Symbols represent individual mice. $^{**}P < 0.01$; NS, not significant.

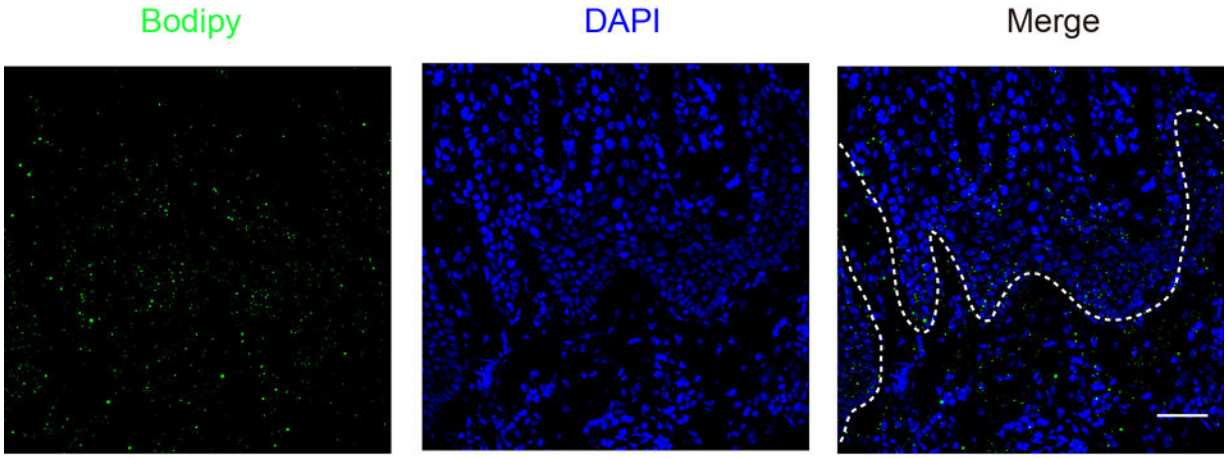

Extended Data Figure 10. Visualization of lipid distribution in human skin from patients with psoriasis by Bodipy staining

Cryosections of lesional scalp skin samples from patients with psoriasis were stained for lipid (4,4-Difluoro-1,3,5,7,8-Pentamethyl-4-Bora-3a,4a-Diaza-s-Indacene (BODIPY 493/503), green) and nuclei (4′,6-diamidino-2-phenylindole (DAPI), blue). Images were acquired with a Leica TCS SP8 confocal microscope and analysed with ImageJ. Dashed lines indicate epidermal–dermal boundary. Scale bar, 50 μm.

Acknowledgments

We thank B. Moss (US National Institute of Health (NIH)) for providing rVACV expressing the OT-I T cell epitope OVA257–264, as well as WR-VACV. This work was supported by NIH grants R01AI041707 (T.S.K.), R01AI127654 (T.S.K.), TR01AI097128 (T.S.K. and R.A.C.) and R01AR063962 (R.A.C.). C.O.P. was supported by a grant of the Korean Health Technology R&D Project, Ministry of Health & Welfare, Republic of Korea (HI14C1799)

References

1. Gebhardt T, et al. Memory T cells in nonlymphoid tissue that provide enhanced local immunity during infection with herpes simplex virus. Nat Immunol. 2009; 10:524–530. [PubMed: 19305395]
2. Masopust D, et al. Dynamic T cell migration program provides resident memory within intestinal epithelium. J Exp Med. 2010; 207:553–564. [PubMed: 20156972]
3. Jiang X, et al. Skin infection generates non-migratory memory CD8$^+$ T_{RM} cells providing global skin immunity. Nature. 2012; 483:227–231. [PubMed: 22388819]

4. Park CO, Kupper TS. The emerging role of resident memory T cells in protective immunity and inflammatory disease. Nat Med. 2015; 21:688–697. [PubMed: 26121195]
5. Clark RA. Resident memory T cells in human health and disease. Sci Transl Med. 2015; 7:269rv1.
6. Ariotti S, et al. Skin-resident memory $CD8^+$ T cells trigger a state of tissue-wide pathogen alert. Science. 2014; 346:101–105. [PubMed: 25278612]
7. Iijima N, Iwasaki A. A local macrophage chemokine network sustains protective tissue-resident memory CD4 T cells. Science. 2014; 346:93–98. [PubMed: 25170048]
8. Schenkel JM, et al. Resident memory CD8 T cells trigger protective innate and adaptive immune responses. Science. 2014; 346:98–101. [PubMed: 25170049]
9. Liu L, et al. Epidermal injury and infection during poxvirus immunization is crucial for the generation of highly protective T cell-mediated immunity. Nat Med. 2010; 16:224–227. [PubMed: 20081864]
10. Gaide O, et al. Common clonal origin of central and resident memory T cells following skin immunization. Nat Med. 2015; 21:647–653. [PubMed: 25962122]
11. Mackay LK, et al. The developmental pathway for $CD103^+CD8^+$ tissue-resident memory T cells of skin. Nat Immunol. 2013; 14:1294–1301. [PubMed: 24162776]
12. Mackay LK, et al. T-box transcription factors combine with the cytokines TGF-β and IL-15 to control tissue-resident memory T cell fate. Immunity. 2015; 43:1101–1111. [PubMed: 26682984]
13. Skon CN, et al. Transcriptional downregulation of *S1pr1* is required for the establishment of resident memory $CD8^+$ T cells. Nat Immunol. 2013; 14:1285–1293. [PubMed: 24162775]
14. Sanz P, Moss B. Identification of a transcription factor, encoded by two vaccinia virus early genes, that regulates the intermediate stage of viral gene expression. Proc Natl Acad Sci USA. 1999; 96:2692–2697. [PubMed: 10077573]
15. Khnykin D, Miner JH, Jahnsen F. Role of fatty acid transporters in epidermis: implications for health and disease. Dermatoendocrinol. 2011; 3:53–61. [PubMed: 21695012]
16. Rogue A, Spire C, Brun M, Claude N, Guillouzo A. Gene expression changes induced by PPAR gamma agonists in animal and human liver. PPAR Res. 2010; 2010:325183. [PubMed: 20981297]
17. Pearce EL, et al. Enhancing CD8 T-cell memory by modulating fatty acid metabolism. Nature. 2009; 460:103–107. [PubMed: 19494812]
18. Pollizzi KN, Powell JD. Integrating canonical and metabolic signalling programmes in the regulation of T cell responses. Nat Rev Immunol. 2014; 14:435–446. [PubMed: 24962260]
19. Hotamisligil GS, Bernlohr DA. Metabolic functions of FABPs—mechanisms and therapeutic implications. Nat Rev Endocrinol. 2015; 11:592–605. [PubMed: 26260145]
20. Maeda K, et al. Role of the fatty acid binding protein mal1 in obesity and insulin resistance. Diabetes. 2003; 52:300–307. [PubMed: 12540600]
21. van der Windt GJW, Chang CH, Pearce EL. Measuring bioenergetics in T cells using a Seahorse extracellular flux analyzer. Curr Protoc Immunol. 2016; 113:16B.1–16B.14. [PubMed: 27038461]
22. Pike LS, Smift AL, Croteau NJ, Ferrick DA, Wu M. Inhibition of fatty acid oxidation by etomoxir impairs NADPH production and increases reactive oxygen species resulting in ATP depletion and cell death in human glioblastoma cells. Biochim Biophys Acta. 2011; 1807:726–734. [PubMed: 21692241]
23. Kantor PF, Lucien A, Kozak R, Lopaschuk GD. The antianginal drug trimetazidine shifts cardiac energy metabolism from fatty acid oxidation to glucose oxidation by inhibiting mitochondrial long-chain 3-ketoacyl coenzyme A thiolase. Circ Res. 2000; 86:580–588. [PubMed: 10720420]
24. Clark RA, et al. The vast majority of CLA^+ T cells are resident in normal skin. J Immunol. 2006; 176:4431–4439. [PubMed: 16547281]
25. Adachi T, et al. Hair follicle-derived IL-7 and IL-15 mediate skin-resident memory T cell homeostasis and lymphoma. Nat Med. 2015; 21:1272–1279. [PubMed: 26479922]
26. Cheuk S, et al. Epidermal Th22 and Tc17 cells form a localized disease memory in clinically healed psoriasis. J Immunol. 2014; 192:3111–3120. [PubMed: 24610014]
27. Zhang Y, et al. Epidermal fatty acid binding protein promotes skin inflammation induced by high-fat diet. Immunity. 2015; 42:953–964. [PubMed: 25992864]

28. O'Sullivan D, et al. Memory CD8$^+$ T cells use cell-intrinsic lipolysis to support the metabolic programming necessary for development. Immunity. 2014; 41:75–88. [PubMed: 25001241]
29. Cui G, et al. IL-7-induced glycerol transport and TAG synthesis promotes memory CD8$^+$ T cell longevity. Cell. 2015; 161:750–761. [PubMed: 25957683]
30. Nomura M, et al. Fatty acid oxidation in macrophage polarization. Nat Immunol. 2016; 17:216–217. [PubMed: 26882249]

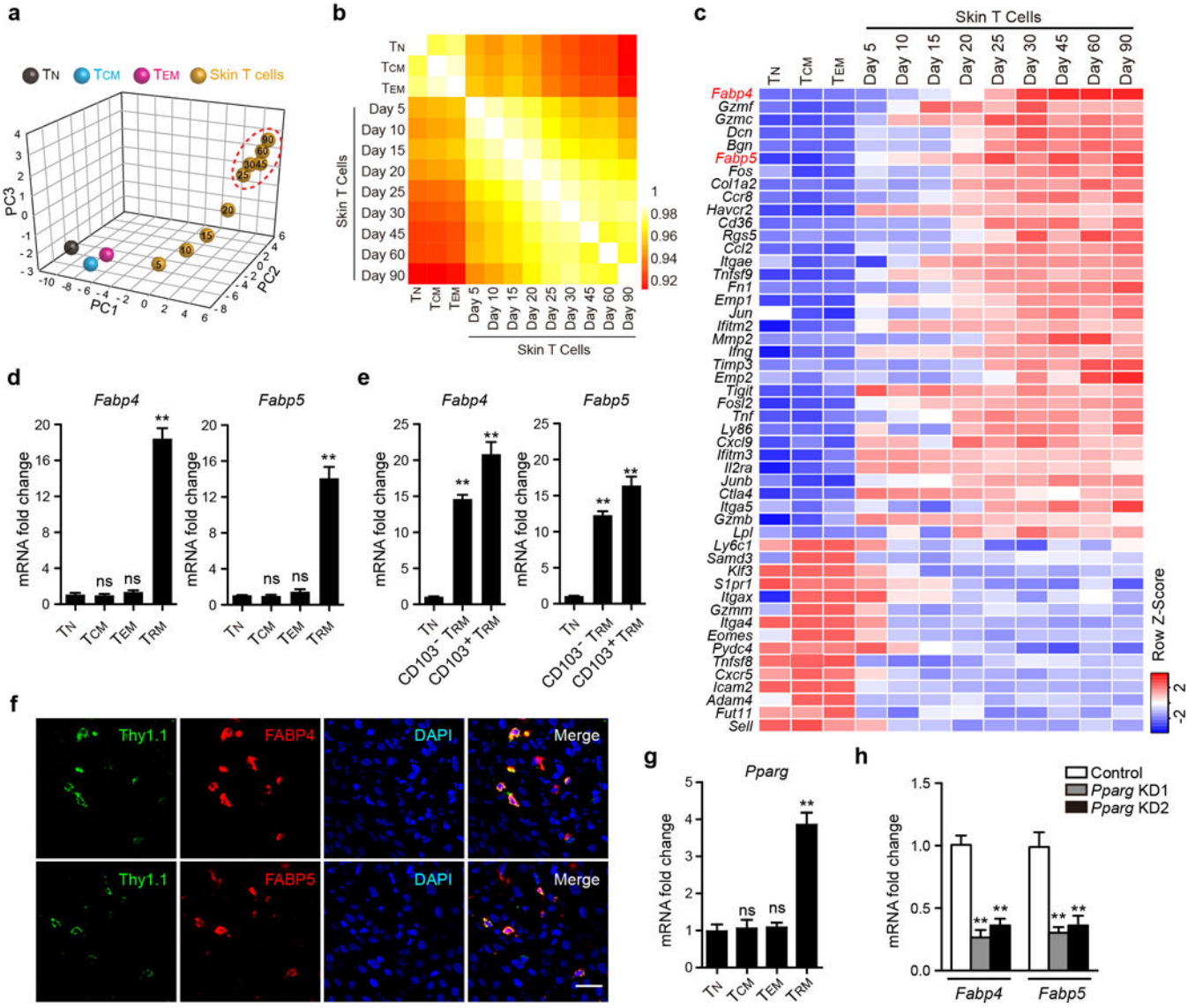

Figure 1. Skin CD8$^+$ T_{RM} cells show increased expression of FABP4 and FABP5

a, Principal-component analysis (PCA) of gene-expression data for CD8$^+$ T cell subtypes. Each time point represents an individual experiment wherein mRNA was pooled from 15–20 mice from 3–4 independent biological groups (5 mice per group). Numbered dots are for skin T cells derived after infection for the indicated number of days. **b**, Pearson correlation coefficients among CD8$^+$ T cell subtypes. **c**, Heatmap of differentially expressed genes selected from a pair-wise comparison between OT-I T_{RM} (day 30) and T_{CM} cells. **d**, qPCR analysis of *Fabp4* and *Fabp5* expression in T_N, T_{CM}, T_{EM} and T_{RM} cells (day 30). **e**, qPCR analysis of *Fabp4* and *Fabp5* gene expression in skin CD103$^-$ and CD103$^+$ T_{RM} cells (day 30). **f**, Immunofluorescence staining of FABP4 (top) and FABP5 (bottom) in OT-I T_{RM} cells 30 days after infection. Scale bar, 20 μm. **g**, qPCR analysis of *Pparg* expression in T_N, T_{CM}, T_{EM} and T_{RM} (day 30). **h**, Effect of lentiviral *Pparg* siRNA knockdown (KD) on *Fabp4* and *Fabp5* expression in OT-I CD8$^+$ T_{RM} cells. Graphs in **d**, **e**, **g**, **h** show mean ± s.d. from triplicates. β-actin was used as internal control and mRNA was normalized to T_N cells (**d**, **e**,

g) or T_{RM} cells transduced with a lentiviral vector encoding scrambled siRNA (**h**). T cells from 15–20 mice were pooled for each group. $^{**}P < 0.01$; NS, not significant.

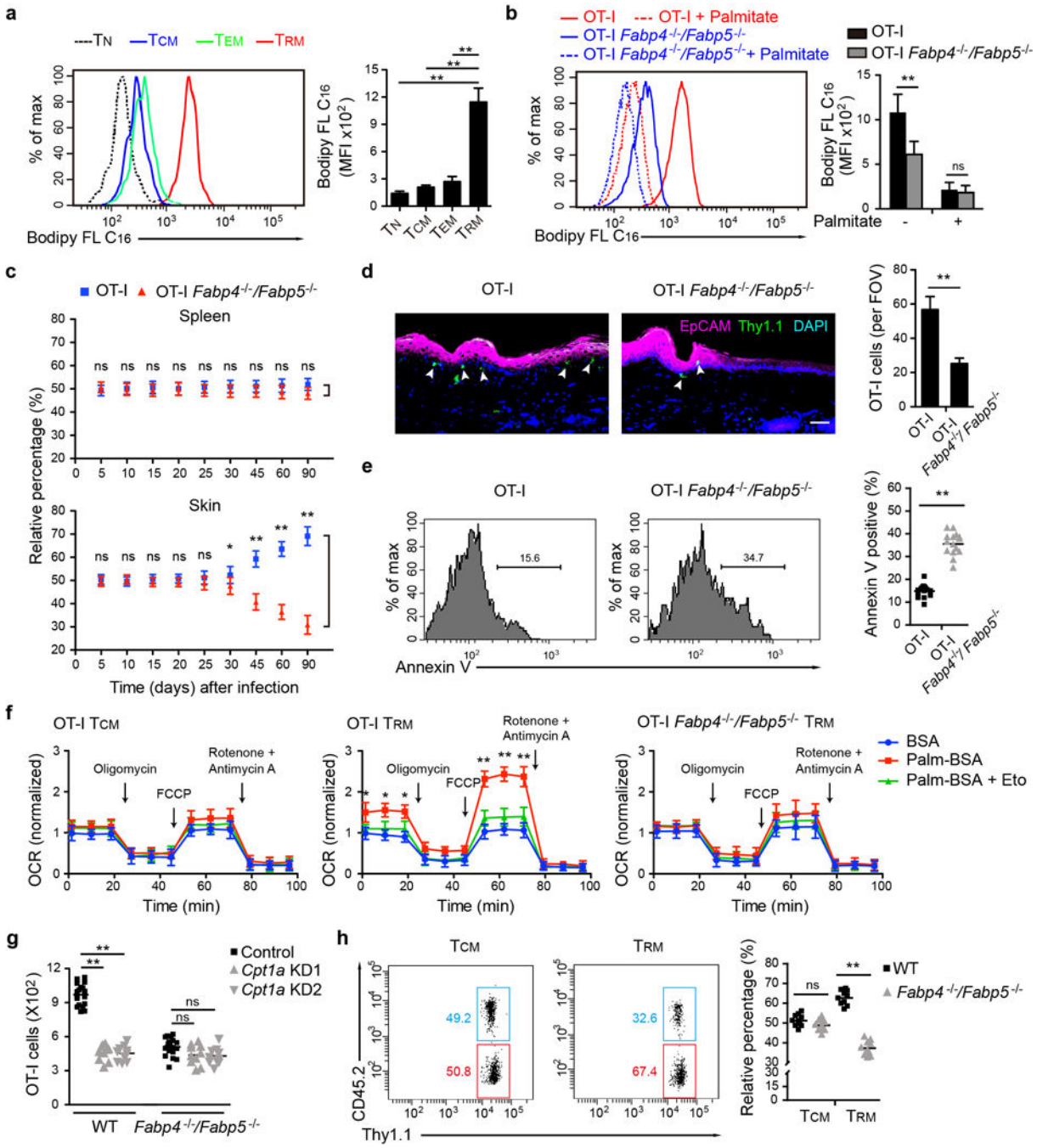

Figure 2. Loss of *Fabp4* and *Fabp5* decreases fatty-acid uptake and metabolism by CD8$^+$ T_{RM} cells and impairs their long-term maintenance

a, Representative histograms and average mean fluorescence intensity (MFI) of Bodipy FL C_{16} uptake by T_N, T_{CM}, T_{EM} or T_{RM} cells (day 30). **b**, Representative histograms and average MFI of Bodipy FL C_{16} uptake in OT-I wild-type and *Fabp4*$^{-/-}$/*Fabp5*$^{-/-}$ T_{RM} cells with or without pre-incubation with unlabelled palmitate (Palm). **c**, Number of OT-I wild-type and *Fabp4*$^{-/-}$/*Fabp5*$^{-/-}$ T_{CM} and T_{RM} cells at different time points after infection in spleen and skin. **d**, Immunofluorescence staining and quantification of OT-I wild-type and

Fabp4$^{-/-}$/*Fabp5*$^{-/-}$ T_{RM} cells at infected skin sites 45 days after infection. FOV, field of view. Scale bar, 50 μm. **e**, Representative histograms and quantification of annexin V^+ cells in OT-I wild-type and *Fabp4*$^{-/-}$/*Fabp5*$^{-/-}$ T_{RM} cells 45 days after infection. **f**, OCR of OT-I T_{CM}, T_{RM} and *Fabp4*$^{-/-}$/*Fabp5*$^{-/-}$ T_{RM} cells (day 30) under basal conditions and in response to indicated mitochondria inhibitors. Results were normalized to control cells treated with bovine serum albumin (BSA). Eto, etomoxir. Graphs show mean ± s.d. of triplicates. **g**, Effect of lentiviral *Cpt1a* siRNA knockdown on OT-I $CD8^+$ T_{RM} survival *in vivo* in infected tissue. **h**, Representative dot plots and percentage of wild-type and *Fabp4*$^{-/-}$/*Fabp5*$^{-/-}$ T_{CM} and T_{RM} cells 45 days after infection. Cells were gated on VACV-specific pentamer$^+$ $CD8^+$ T cells. Graphs show mean ± s.d. of 5 (**a**, **b**) or 10 (**c**) mice, or 50 fields from 5 mice (**d**, 10 fields per mouse), or symbols represent individual mice (**e**, **g**, **h**). *P <0.05; **P < 0.01; NS, not significant.

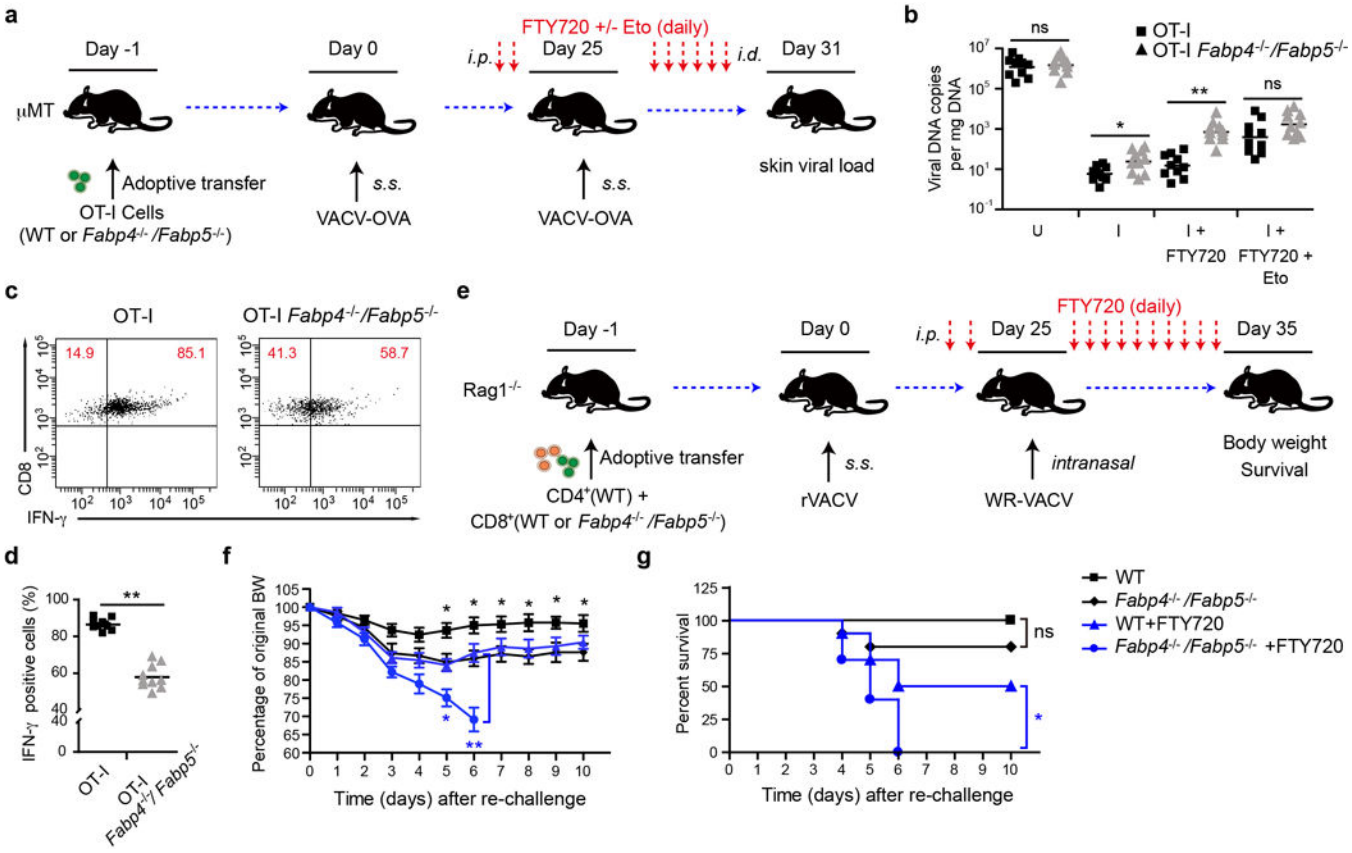

Figure 3. Skin *Fabp4*$^{-/-}$/*Fabp5*$^{-/-}$ CD8^{+} T$_{RM}$ cells fail to protect mice against viral infectious challenge

a, Schematic of experimental design. i.p., intraperitoneal injection; s.s., **b**, qPCR analysis of skin viral load at six days after re-infection. U, un-immunized mice; I, immunized mice. **c**, **d**, Representative dot plots and quantification of IFNγ secretion by OT-I wild-type or *Fabp4*$^{-/-}$/*Fabp5*$^{-/-}$ T$_{RM}$ cells. Symbols represent individual mice (**b**, **d**). **e**, Schematic of experimental design. **f**, **g**, Body weight (BW) (**f**) and survival measurements (**g**) of WR-VACV challenged mice, with or without FTY720 treatment. Data are representative of three independent experiments (n = 10 mice per group). *P < 0.05; **P < 0.01; NS, not significant.

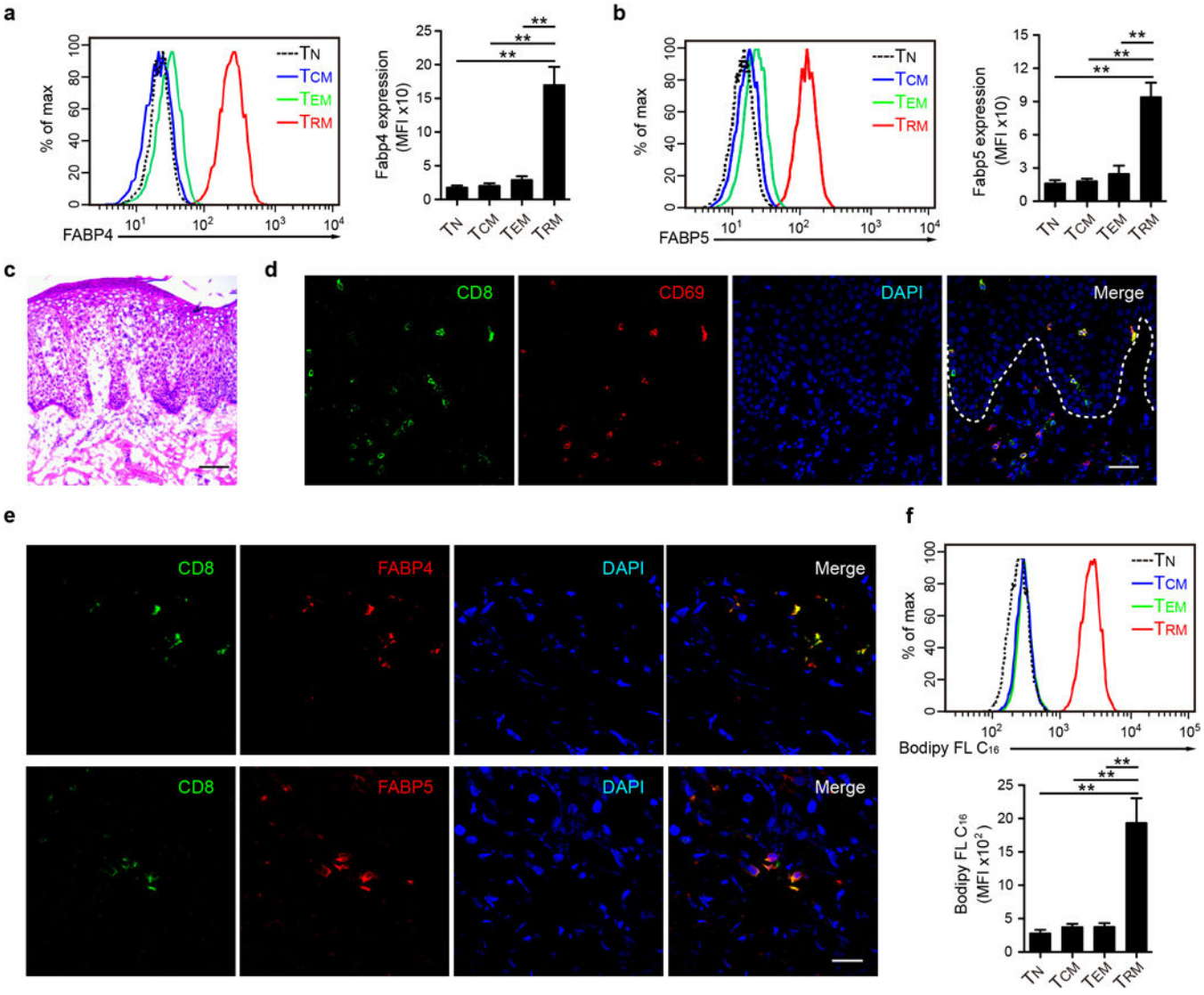

Figure 4. Human skin CD8$^+$ T_{RM} demonstrate increased expression of FABP4 and FABP5

a, b, Representative histograms and average MFI of intracellular staining of FABP4 (**a**) and FABP5 (**b**) in human peripheral blood mononuclear T_N, T_{CM}, and T_{EM} cells compared to facial skin T_{RM}. **c**, Haematoxylin and eosin staining of a human psoriatic lesion. Scale bar, 100 μm. **d**, Immunofluorescence staining of CD8 and CD69 expression in psoriatic human skin. Dashed line indicates epidermal–dermal junction. Scale bar, 50 μm. **e**, Immunofluorescence staining of FABP4 (top) and FABP5 (bottom) expression in skin CD8$^+$ T_{RM} cells from patients with psoriasis. Scale bar, 20 μm. **f**, Representative histograms and average MFI of Bodipy FL C_{16} uptake by human T_N, T_{CM}, T_{EM} or T_{RM} cell subsets. **a**, **b**, **f**, Graphs show mean ± s.d. of 5 individuals; **c**–**e**, Representative images of $n = 15$ sections from 5 individuals. $^{**}P < 0.01$.